JCI insight

Distinct glutamatergic projections of the posteroventral medial amygdala play different roles in arousal and anxiety

Ying Li, … , Linlin Bi, Haibo Xu

JCI Insight. 2024. https://doi.org/10.1172/jci.insight.176329.

Research In-Press Preview Neuroscience

Graphical abstract

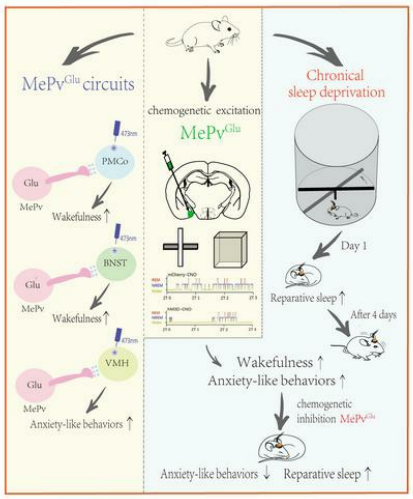

Find the latest version:

https://jci.me/176329/pdf

Distinct glutamatergic projections of the posteroventral medial amygdala play different roles in arousal and anxiety

Short title: The role of MePV in arousal and anxiety

Ying Li[1,#], Yuchen Deng[1,#], Yifei Zhang[2,3,#], Dan Xu[4], Xuefen Zhang[1], Yue Li[1], Yidan Li[1], Ming Chen[5], Yuxin Wang[2,3], Jiyan Zhang[2,3], Like Wang[2,3], Yufeng Cang[2,3], Peng Cao[7,8]*, Linlin Bi[2,3,6]*, Haibo Xu[1]*.

[1] Department of Radiology, Zhongnan Hospital of Wuhan University, Wuhan University, Wuhan, 430071, China.

[2] Department of Pathology, Taikang Medical School (School of Basic Medical Sciences), Wuhan University, Wuhan, 430071, China.

[3] Center for Pathology and Molecular Diagnostics, Zhongnan Hospital of Wuhan University, Wuhan University, Wuhan, 430071, China.

[4] Department of Nuclear Medicine, Zhongnan Hospital of Wuhan University, Wuhan University, Wuhan 430071, China.

[5] Department of Cardiology, Zhongnan Hospital of Wuhan University, Wuhan University, 430071, China.

[6] Guangdong Province Key Laboratory of Psychiatric Disorders, Southern Medical University, Guangzhou, 510515, China.

[7] National Institute of Biological Sciences, Beijing, China.

[8] Tsinghua Institute of Multidisciplinary Biomedical Research, Tsinghua University, Beijing, China

*Corresponding authors' E-mail(s): caopeng@nibs.ac.cn; linlinbi2016@whu.edu.cn; xuhaibo@whu.edu.cn

[#] These authors contributed equally to this work.

Abstract

Sleep disturbance usually accompanies anxiety disorders and exacerbates their incidence rates. The precise circuit mechanisms remain poorly understood. Here, we found that glutamatergic neurons in the posteroventral medial amygdala ($MePV^{Glu}$) are involved in arousal and anxiety-like behaviors. Excitation of $MePV^{Glu}$ neurons not only promoted wakefulness but also increased anxiety-like behaviors. Different projections of $MePV^{Glu}$ neurons played various roles in regulating anxiety-like behaviors and sleep-wakefulness. $MePV^{Glu}$ neurons promoted wakefulness through the $MePV^{Glu}$-posteromedial cortical amygdaloid area (PMCo) pathway and the $MePV^{Glu}$-bed nucleus of the stria terminals (BNST) pathway. In contrast, $MePV^{Glu}$ neurons increased anxiety-like behaviors through the $MePV^{Glu}$-ventromedial hypothalamus (VMH) pathway. Chronic sleep disturbance increased anxiety levels and reduced reparative sleep, accompanied by the enhanced excitability of $MePV^{Glu}$-PMCo and $MePV^{Glu}$-VMH circuits but suppressed responses of glutamatergic neurons in the BNST. Inhibition of the $MePV^{Glu}$ neurons could rescue chronic sleep deprivation-induced phenotypes. Our findings provide important circuit mechanisms for chronic sleep disturbance-induced hyperarousal response and obsessive anxiety-like behavior, and are expected to provide a promising strategy for treating sleep-related psychiatric disorders and insomnia.

Keywords: MePV, glutamatergic neurons, sleep, wake, anxiety

Teaser: Amygdala-related important circuit mechanisms for abnormal sleep architecture and anxiety disorders

Introduction

Moderate vigilance and fear in the face of threats can help animals quickly detect danger and wake up from sleep. However, hyperarousal response and obsessive anxiety-like behavior are involved in several adverse sleep architectural changes (1, 2). Stress, such as a physical or emotional stimulus, can cause disrupted or shortened sleep (3, 4). Some patients with anxiety disorders often exhibit hyperarousal responses to sensory stimuli (5). Furthermore, the presence of sleep disturbances has been found to exacerbate the risk of developing anxiety disorders (1, 6). Passive sleep deprivation could worsen anxiety disorders and cause changes in the structure of sleep, but little research has been done on the mechanisms by which sleep deprivation impairs the emotion and sleep systems. Elucidating the neural circuits that control physiological arousal to detect threats is imperative to understanding maladaptive emotional states and abnormal sleep changes.

The medial amygdala (Me) is a critical brain region that encodes fear-related behavior (7, 8). The Me is composed of several subnuclei with differing structures and functions, such as the posterodorsal (MePD), posteroventral (MePV), and anterior (MeA) (9-11). Most MePD neurons are GABAergic, whereas many MeA/PV ones are glutamatergic (9-11). MePV cells that project to the ventromedial hypothalamus (VMH) are glutamatergic neurons and increase their activity in response to cat odor in mice (12). Previous studies have shown that MePV and paraventricular hypothalamic nucleus (PVN) upregulated c-fos expression when rats were exposed to cat odor (13). In the present study, we focused on the function of the MePV.

The posteroventral component of the medial amygdaloid nucleus (MePV) was found to be implicated in coping with inherent danger cues by utilizing activity mapping of the immediate-early gene c-fos (12, 14). In mice, the MePV is triggered when a natural danger stimulus approaches (15). Distinct subpopulations of MePV neurons project to the bed nucleus of the stria terminals (BNST) and the VMH in different ways. These projections have opposing consequences on investigating or avoiding potentially dangerous stimuli (15). Previous research demonstrated that VMH outputs play a role in modulating anxiety-like behavior and fear (16). Results from an open-field experiment (8) revealed that VMH neurons expressing the nuclear receptor protein NR5A1 (also known as SF1) in mice displayed sustained activity encountering stimuli necessary for persistent protective behavior, indicating that MePV-VMH has a putative function in controlling anxiety-like behaviors. Although BNST is involved in the modulation of anxiety-like behaviors and fast changes in arousal (17), the effect of projecting MePV neurons to the BNST on the regulation of arousal or anxiety remains unclear.

A previous study suggested that the posteromedial cortical amygdaloid area (PMCo) might regulate social odour and primary olfactory processing (18). Although the authors revealed the connectivity of the PMCo feedback circuit innervating the mouse accessory olfactory bulb (18-20), the functions of PMCo on wakefulness-sleep or anxiety were barely reported. Although our preliminary data revealed an increase in PMCo activity by the chemogenetic excitation of MePV neurons, the role of MePV→PMCo in wake-sleep or anxiety was unknown. Therefore, we hypothesized that the MePV→PMCo, MePV→VMH pathway, or MePV→BNST pathway might be important gates for controlling responses to threatening stimuli or physiological arousal. Further research exploration is needed to elucidate cell-type and circuit-specific features in the MePV that control the integration of stress and sleep-wake.

Previous research has shown that glutamatergic neurons in other brain areas, such as the paraventricular hypothalamic nucleus (PVN), can control anxiety and arousal (21). Given MePV's role in regulating innate defensive responses, coupled with the fact that MePV neurons are mainly glutamatergic (9, 11, 17) and that downstream brain region BNST is involved in arousal behaviors, we hypothesized that glutamatergic neurons in the MePV are potentially involved in regulating anxiety-like behaviors and arousal response to threatening stimuli. In the present study, we employed *in-vivo* calcium imaging and cell-type-specific manipulations to reveal that neural circuits involving $MePV^{Glu}$ neurons not only regulate both anxiety-like behaviors and sleep-wakefulness, but also control the sleep deprivation-mediated obsessive anxiety-like behavior and sleep change. We also investigated the downstream neural networks and underlying processes for modulating responses to hazardous stimuli or physiological arousal.

Results

$MePV^{Glu}$ neurons were selectively active during threat-evoked wake from Non-rapid Eye Movement (NREM) sleep

To check whether endogenous $MePV^{Glu}$ neurons are involved in the regulation of the natural sleep-wake cycle or anxiety-like behaviors, we injected AAV-CaMKIIa-GCaMP6f into the MePV of C57 mice ($MePV^{Glu}$-GCaMP6f mice) and recorded changes in Ca^{2+} signal during sleep state transitions using the EEG-EMG system or anxiety state transitions during behavioral tests (Fig. 1A). On the elevated plus maze test, the level of Ca^{2+} signal increased when mice approached the open arms and dropped when mice returned to the closed arms from the open arms (Fig. 1B, C). Subsequently, the loud noise of opening the soundproofed door of the recording chamber was used to simulate the intruder's stimuli while

capturing the Ca^{2+} signal (to make this experiment consistent every time, the noises of 25-30dB measured by a sound decibel meter were selected). The Ca^{2+} signal increased dramatically from NREM to threat-evoked waking and from NREM to Rapid Eye Movement (REM) sleep (Fig. 1D, E). In addition to this, we also explored the alterations of neuronal Ca^{2+} signals in mice that were forced to wake up under other stimulating conditions (Supplementary Fig. 2B, C). It was found that the △F/F ratio increased from NREM to threat-evoked wake and from NREM to REM (Fig. 1D, E) but dropped from REM to natural wake (Fig. 1F). The △F/F ratio increased when mice were forced to wake up with alcohol spraying (Supplementary Fig. 2B) or 90db white noise stimulation (Supplementary Fig. 2C). The results showed that the Ca^{2+} signal of $MePV^{Glu}$ neurons changed significantly when they were forced to wake up. The change in △F/F ratio was minimal throughout the transition from NREM to natural wake (Fig. 1G). During the microarousal stage, which occurred during sleep, the △F/F ratio decreased (Fig. 1H, I). Endogenous $MePV^{Glu}$ neurons were found to respond to threatening situations, threat-evoked wakefulness, and microarousal but not in natural wakefulness.

Chemogenetic excitation of $MePV^{Glu}$ neurons promoted wakefulness and increased anxiety-like behaviors

Although endogenous $MePV^{Glu}$ neurons may not be involved in calm sleep and awake, over-excited $MePV^{Glu}$ neurons can potentially be involved in stress-induced hyperarousal as suggested by the above research. However, whether the increased Ca^{2+} signal of $MePV^{Glu}$ neurons when mice entered the open arms triggered obsessive anxiety-like behavior or exploration-related behaviors was still uncertain. Using the bilateral expression of excitatory hM3Dq receptors that were specifically induced by clozapine N-oxide (CNO), the behavioral effect of chemogenetic activation of $MePV^{Glu}$ neurons was examined. Three weeks after the viral injection, a histological examination was conducted to confirm hM3Dq-mCherry expression, particularly in $MePV^{Glu}$ neurons (Fig. 2A).

We first proved that MePV neurons in the $MePV^{Glu}$-hM3Dq mice were excited by CNO. 1h after CNO or saline i.p. injection into $MePV^{Glu}$-hM3Dq mice, activated neurons (cFOS-positive) were significantly increased in the CNO group compared with that in the control group (Fig. 2B and Supplementary Fig. 3). After the CNO treatment (1 mg/kg, i.p. injection), the wakefulness remained elevated for 3h. Both NREM sleep and REM sleep were decreased by the CNO treatment (Fig. 2C, D, E). As a control for the specificity of CNO's actions, we injected AAV-CaMKIIa-mCherry into the MePV of C57 mice; CNO injection (i.p.) into these $MePV^{Glu}$ -mCherry mice did not affect sleep or wakefulness time (Fig. 2C, D, E). Typical examples of hypnogram, EMG track, EEG track, and EEG spectrogram for 3h from $MePV^{Glu}$-hM3Dq mice respectively given saline or CNO (i.p., 1 mg/kg) were shown in Supplementary Fig. 8A, B.

Stimulation of $MePV^{Glu}$ neurons did not result in hyperactivity. Moreover, the locomotion of CNO-injected mice was not significantly different from that of saline-injected mice in the open field test. Further, chemogenetic stimulation of $MePV^{Glu}$ neurons reduced the time spent in the center in the open field test (Fig. 2F). The CNO injection increased the time spent on the closed arms while decreasing the time spent on the open arms on the elevated plus maze (Fig. 2G). Overall, these results suggest that chemogenetic stimulation of $MePV^{Glu}$ neurons might increase wakefulness and anxiety-like behaviors but does not influence locomotion.

To test whether the MePV functions of female mice and male mice were different, we injected AAV-CaMKII-hM3Dq-mCherry virus and AAV-CaMKII -mCherry virus into $MePV^{Glu}$ neurons of female mice and implanted EEG-EMG electrodes (Supplementary Fig. 4A). After three weeks of recovery, Same as males, NREM sleep of females was decreased by the CNO treatment (Supplementary Fig.4B). The

CNO injection increased the time spent on the closed arms while decreasing the time spent on the open arms on the elevated plus maze (Supplementary Fig. 4C, E). Chemogenetic stimulation of MePV^{Glu} neurons slightly reduced the time spent in the center in the open field test (Supplementary Fig. 4D, F). Overall, these results suggested that MePV^{Glu} neurons played a similar role in regulating sleep and anxiety-like behaviors in both female and male mice.

Optogenetic excitation of MePV glutamatergic neurons promoted wakefulness and increased anxiety-like behaviors

To further prove that mice relied on MePV^{Glu} neurons to regulate anxiety-related behaviors or to govern arousal behaviors during NREM sleep and waking states, we next tested whether optogenetic activation of MePV^{Glu}-Channelrhodopsin 2 (ChR2) expressing neurons influenced wakefulness and anxiety-like behavior.

After injecting the AAV-CaMKIIa-hChR2-GFP virus into the MePV, we implanted optical fibers into the MePV to produce MePV^{Glu}–ChR2 mice (Fig. 3A). Functional expression of ChR2 was validated using *in-vitro* electrophysiology (Fig. 3B). Optogenetic stimulation of CaMKIIa-ChR2–expressing neurons triggered the firing of action potentials of glutamatergic neurons (Fig. 3B). During the light phase, we applied optical stimulation at the time of stable NREM sleep until the onset of wakefulness. The latency was defined as the optical stimulation time before the onset of wakefulness. Optogenetic stimulation of the MePV^{Glu}-ChR2 neurons promoted waking from NREM sleep (Fig. 3C). The latencies of NREM to wake were gradually reduced by the higher light stimulation frequencies of 5Hz, 10Hz, 15Hz, and 20Hz, respectively (Fig. 3D). In addition, long-term optogenetic stimulation for 2h increased wakefulness and reduced NREM and REM sleep (Fig. 3E, F, G). Typical examples of the hypnogram, EMG track, EEG track, and EEG spectrogram for ZT0–ZT6 from the MePV^{Glu}-GFP mice and the MePV^{Glu}-ChR2 mice are shown in Supplementary Fig. 9A and 9B, respectively.

No hyperactivity was caused by optogenetic stimulation of MePV^{Glu}-ChR2 expressing neurons, consistent with the impact of chemogenetic activation of MePV^{Glu} neurons. The locomotion distance was not substantially different between the light-ChR2 group and the control group in the open field test (Fig. 3H). The light-induced activation of MePV^{Glu}-ChR2 neurons increased the time spent on the closed arms and reduced the time spent on the open arms on the elevated plus maze (Fig. 3I). Overall, optogenetic activation of MePV^{Glu} neurons could increase wakefulness and anxiety-like behaviors.

MePV glutamatergic neurons promoted wakefulness through the MePV^{Glu}-PMCo pathway

Measuring the track of viral expression and c-fos activity in MePV^{Glu}-hM3Dq mice allowed targeting of the brain circuits responsible for MePV^{Glu}-mediated wakefulness. Numerous brain areas showed high c-fos-positive neurons following the CNO i.p. injection. Particularly, c-fos expression was seen in the PMCo (Supplementary Fig. 5). CNO infusion increased the number of c-fos-expressing neurons than saline injection (Supplementary Fig. 5). The circuit connections of MePV^{Glu} neurons in the MePV^{Glu}-ChR2-GFP mice were mapped. There was a dense projection of MePV^{Glu} neurons to the PMCo, consistent with the results above (Supplementary Fig. 6). Following optogenetic activation of MePV^{Glu} neuron axons ending in the PMCo, light-evoked excitatory postsynaptic currents (eEPSCs) were found in PMCo neurons using whole-cell electrophysiological recordings in brain slices (Fig. 4B).

AAV-CaMKIIa-hChR2-GFP virus was injected into the MePV, and optical fibers were implanted into the PMCo to stimulate the terminals of MePV^{Glu} neurons to examine whether activation of MePV^{Glu} PMCo projections could enhance wakefulness or promote anxiety-like behaviors (Fig. 4A). We found that optogenetic stimulation of MePV^{Glu} terminals in the PMCo facilitated awakening from NREM sleep.

The latencies of NREM sleep to wake decreased with an increase in stimulation frequencies (Fig. 4C, D). 2h optogenetic stimulation enhanced alertness while decreasing REM and NREM sleep (Fig. 4E, F, G). Typical examples of the hypnogram, EMG track, EEG track, and EEG spectrogram for ZT0-ZT6 from MePV^{Glu}-ChR2 mice and MePV^{Glu}-GFP are displayed in Supplementary Fig. 10A and 10B.

Optogenetic activation of the MePV^{Glu} terminals in the PMCo caused hyperactivity. The locomotion distance of the light-ChR2 group was considerably more than that of the baseline-ChR2 group in the open field test (Fig. 4H). The light stimulation of MePV^{Glu} terminals in the PMCo enhanced the time spent on the open arms of the raised plus maze (Fig. 4I). As a result, the MePV^{Glu}-PMCo pathway is a crucial functional neural circuit that regulates wakefulness, movement, and anxiety-like behaviors. Activation of the MePV^{Glu}-PMCo pathway increased wakefulness, induced anxiolytic effects, and promoted locomotion.

MePV^{Glu} neurons promoted wakefulness via the MePV^{Glu}-BNST pathway

Dense green fluorescence nerve fiber tracts were observed in the BNST area on the MePVGlu-ChR2-GFP labeled circuit map (Supplementary Fig. 6). To test whether MePV^{Glu}→BNST projections could regulate wakefulness or anxiety-like behaviors, we injected AAV-CaMKIIa-hChR2-GFP into the MePV and implanted optical fibers into the BNST to stimulate the fluorescence nerve fiber terminals (Fig. 5A). Light-stimulated excitatory postsynaptic currents (eEPSCs) were found in BNST neurons after optogenetic activation of MePV^{Glu} neuronal terminals in the BNST using whole-cell electrophysiological recordings in brain slices (Fig. 5B).

Optogenetic stimulation of the MePV^{Glu}-BNST nerve fiber terminals promoted wakefulness from NREM sleep. On the other hand, the latencies of NREM-to-wake were shortened by the high stimulation frequencies (Fig. 5C, D). Two hours of prolonged optogenetic stimulation enhanced wakefulness and reduced REM and NREM sleep (Fig. 5E, F, G). Typical examples of the hypnogram, EMG track, EEG track, and EEG spectrogram for ZT0–ZT6 from the MePV^{Glu}-GFP mice and the MePV^{Glu}-ChR2 mice are shown in Supplementary Fig. 11A and 11B, respectively.

However, optogenetic activation of the MePV^{Glu} terminals in the BNST showed no significant impact on the elevated plus maze or open-field test (Fig. 6H, I). No significant difference was observed in the locomotion distance or time spent in the center between the light-ChR2 group and the baseline-ChR2 group in the open field test (Fig. 4H). The light stimulation of MePV^{Glu} terminals in the BNST had no impact on how much time was spent on the open or closed arms of the elevated plus maze (Fig. 6H, I). In all, the MePV^{Glu}-BNST route was crucial for regulating wakefulness but not anxiety-like behaviors.

MePV^{Glu} neurons increased anxiety-like behaviors via the VMH area

As shown in the MePV^{Glu}-ChR2-GFP labeled circuits, some green fluorescence nerve fiber tracts were also found in the VMH area. To test whether MePV^{Glu}→ VMH projections could regulate wakefulness or anxiety-like behaviors, we injected the AAV-CaMKIIa-hChR2-GFP virus into the MePV and placed optical fibers into the VMH to stimulate the fluorescence nerve fiber tracts (Fig. 6A). Light-evoked EPSCs were found in VMH neurons after optogenetic activation of MePV^{Glu} neuronal terminals using whole-cell path recordings in brain slices (Fig. 6B).

Optogenetic stimulation of the MePV^{Glu}→ VMH nerve fiber terminals had no significant effect on wakefulness from NREM sleep (Fig. 6C, D). Long-term optogenetic stimulation of this pathway for 2h didn't affect sleep and wakefulness (Fig. 6E, F, G). Typical examples of the hypnogram, EMG track, EEG track, and EEG spectrogram for ZT0–ZT6 from the MePV^{Glu}-GFP mice and the MePV^{Glu}-ChR2 mice are shown in Supplementary Fig. 12A and 12B, respectively.

Optogenetic stimulation of the MePV^{Glu}→ VMH fluorescence nerve fiber terminals decreased the

locomotion and reduced the time spent in the center of the open field test (Fig. 6H). Optogenetic activation of the MePV^{Glu}-VMH pathway reduced time spent on the open arms and increased time spent on the closed arms during the elevated plus maze test (Fig. 6I). Thus, the MePV^{Glu} -VMH pathway was an important neuronal circuit for regulating anxiety-like behaviors but not for the modulation of sleep and wakefulness.

There were no interactions between different downstream projections of MePV^{Glu} neurons

Although we had explored the role of different downstream projections of MePV^{Glu} in wakefulness and anxiety, it was still unclear whether there were reciprocal projections between downstream neurons and whether MePV^{Glu} neurons could cause back propagation resulting in cell body activation.

In order to find out the above questions, we injected AAV-CaMKIIa-hChR2-mCherry into the MePV. We also injected rAAV-CaMKIIa-GCaMP6f into the BNST, PMCo, and VMH to record the activity of glutamatergic neurons (Supplementary Fig. 7) and implanted optical fibers into BNST, PMCo, and VMH to activate the terminals of MePV neurons. After 4 weeks of recovery in the mice, we delivered blue light stimulation (10 Hz, 10 mW, 473 nm, 1s blue light stimulation at 50s intervals) into the terminals of MePV in the BNST. We recorded changes in the Ca^{2+} signal in the remaining two downstream regions, PMCo and VMH. The same light stimulation was delivered into the PMCo and VMH, and changes in Ca^{2+} signal in the other two downstream regions were recorded. We found that all Ca^{2+} signal was not significantly changed when the laser was delivered into the terminals of MePV neurons in the BNST, PMCo, or VMH (Supplementary Fig. 7). These results suggested that there were no reciprocal projections between downstream neurons and high frequency stimulation of terminals might not cause back propagation resulting in cell body activation in our research.

Inhibiting MePV^{Glu} neurons with a chemogenetic agent induced an anxiolytic effect without affecting natural sleep and wakefulness

The above results suggest that the endogenous MePV^{Glu} neurons might be related to the hyper-arousal response and anxiety-like behaviors. To investigate whether inhibiting the endogenous MePV^{Glu} neurons could affect sleep or anxiety-like behaviors, we developed MePV^{Glu}-hM4Di mice, of which MePV^{Glu} neurons were suppressed by injecting saline or CNO (i.p., 1 mg/kg) (Fig. 7A).

We recorded and examined EEG and EMG data following saline or CNO (i.p., 1 mg/kg) injections (Fig. 7A). However, sleep or wakefulness of the MePV^{Glu}-hM4Di mice was unaffected by CNO injection. AAV-CaMKIIa-mCherry was injected into the MePV as an additional control for the specificity of the effect of CNO. CNO injection into these MePV^{Glu} -mCherry mice had no effect on undisturbed sleep or wakefulness (Fig. 7C, D, E). Typical examples of the hypnogram, EMG track, EEG track, and EEG spectrogram for 3h from the MePV^{Glu}-hM4Di mice are displayed in Supplementary Fig. 13A and 13B. These findings revealed that sleep and wakefulness were unaffected by the suppression of endogenous MePV^{Glu} neurons.

We next performed behavioral tests and found that inhibiting MePV^{Glu} neurons had no effect on the locomotion distance and speed in the open field test. However, the CNO-injected mice spent more time in the center in the open field test than the control group (Fig. 7F). The CNO treatment could also enhance open-arm time and reduce the closed-arm time on the elevated plus maze test. Therefore, inhibition of the MePV glutamatergic neurons reduced anxiety-like behaviors (Fig. 7G). All these results suggested that the endogenous MePV^{Glu} neurons regulated anxiety-related behaviors but might not be involved in the undisturbed sleep and wakefulness of normal mice. These results indicated that MePV^{Glu} neurons could be potential targets for treating anxiety disorders.

Sleep deprivation (SD) increased the activity of MePV neurons and changed the excitability of the MePV-related neuronal circuits.

The above results suggest that though endogenous MePV^{Glu} neurons might not be involved in undisturbed sleep-wake transitions, the endogenous MePV^{Glu} neurons might be related to sleep disruption and anxiety disorders. As we know, chronic passive sleep disturbance could worsen anxiety disorders and change the structure of sleep, but little research has been done on the mechanisms. We then first tested the effect of chronic sleep deprivation on the activity of MePV neurons and MePV-related neuronal circuits using c-fos immunohistochemical staining. Numerous brain areas showed high c-fos-positive neurons following sleep deprivation. Notably, sleep deprivation significantly increased the number of c-fos-expressing neurons in the MePV, VMH, and PMCo areas (Fig. 8A-8C and Supplementary Fig14). However, sleep deprivation didn't significantly affect the number of c-fos-expressing neurons in the BNST area compared with the control group (Fig. 8D and Supplementary Fig14).

To test whether chronic sleep deprivation affected the real-time activity of MePV neurons and neuronal circuits, we injected AAV-CaMKIIa-hChR2-mCherry into the MePV and implanted optical fibers into MePV to activate the MePV neurons. We also injected rAAV-CaMKIIa-GCaMP6f into the BNST, PMCo and VMH to record the activity of glutamatergic neurons (Fig. 8). We found that the level of Ca^{2+} signal in the BNST, PMCo and VMH all increased when the laser was delivered into the MePV(Fig. 8E, 8F and 8G). Compared with the control group, sleep deprivation significantly increased the laser-evoked Ca^{2+} signal of glutamatergic neurons in the PMCo and VMH groups (Fig. 8E and 8F). But the sleep deprivation significantly decreased the laser-evoked Ca^{2+} signal of glutamatergic neurons in the BNST group (Fig. 8G). All these results suggested that chronic sleep deprivation increased the activity of MePV glutamatergic neurons and changed the excitability of the downstream circuits. We then hypothesized that MePV glutamatergic neurons might participate in chronic sleep deprivation-induced abnormal changes in anxiety and sleep.

Inhibiting MePV^{Glu} neurons with a chemogenetic agent decreased wakefulness and induced an anxiolytic effect on the mice treated with SD.

To investigate whether chronic sleep deprivation could affect sleep and anxiety-like behaviors, or whether inhibiting the endogenous MePV^{Glu} neurons could reverse the effect of sleep deprivation, we developed MePV^{Glu}-hM4Di mice, of which MePV^{Glu} neurons were suppressed by injecting saline or CNO (i.p., 1 mg/kg) (Fig. 9A, and 9B). We subjected the mice to five days of sleep deprivation, and recorded and examined EEG and EMG data for 6 hours immediately after the sleep deprivation every day(Fig. 9C). We found that 1 day of sleep deprivation significantly decreased wakefulness, increased NREM sleep and REM sleep (Fig. 9C). Because the mice were forced to stay awake during the sleep deprivation, the increased sleep after the sleep deprivation on Day1 was reparative. But from the 2nd day on, the wakefulness increased and NREM sleep decreased (Fig. 9C), which suggested that the mice experienced a significant reduction in reparative sleep, and had a relative increase in total wakefulness and a relative decrease in NREM sleep duration. On the 6th day after the sleep deprivation, we injected CNO (i.p., 1 mg/kg) to inhibit the MePV^{Glu} neurons, and found that the CNO treatment significantly decreased the wakefulness time of the SD group compared with the non-SD group (Fig. 9C and 9D). The NREM sleep of the SD group was significantly increased by the CNO treatment compared with that of the no-SD group (Fig. 9C, and 9D). 5 days of sleep deprivation increased the REM sleep (Fig. 9C and 9D), but the CNO treatment didn't affect the REM sleep time in both the non-SD group and the SD group (Fig. 9C, and 9D).

To study the effects of sleep deprivation on the activity of MePV^{Glu} neurons, we recorded the Ca^{2+}

signals of MePV^{Glu} neurons from NREM to arousal transitions after one day or five days of sleep deprivation, respectively (Supplementary Fig. 2 E, F). After the first day of sleep deprivation, the Ca^{2+} signal of MePV^{Glu} neurons was decreased during NREM-wake transitions (Supplementary Fig. 2 E). However, five days after sleep deprivation, the Ca^{2+} signal of MePV^{Glu} neurons was increased during NREM-wake transitions (Supplementary Fig. 2 F). All these results suggested that the decreased activity of MePV^{Glu} neurons during NREM-wake transitions caused a rebound of NREM sleep on Day 1, and SD-mediated increased activity of MePV^{Glu} neurons during NREM-wake transitions might promote wakefulness after chronic sleep deprivation.

We next performed behavioral tests and found that inhibiting MePV^{Glu} neurons of the SD group didn't affect the locomotion in the open field test compared with the saline group. However, the CNO-injected mice spent more time in the center in the open field test than the SD-saline group (Fig. 9E). The CNO treatment after the sleep deprivation could also increase open-arm time and decrease the closed-arm time in the elevated plus maze test compared with the SD-saline group (Fig. 9F). Therefore, inhibition of the MePV^{Glu} neurons reduced anxiety-like behaviors after chronic sleep deprivation. All these results suggested that the endogenous MePV^{Glu} neurons might be involved in sleep deprivation-mediated obsessive anxiety-like behavior and sleep change. Inhibition of the MePV^{Glu} neurons reduced anxiety-like behaviors after sleep deprivation and promoted restorative sleep. These results indicated that MePV^{Glu} neurons could be potential targets for treating anxiety disorders and insomnia.

Discussion

Exposure to threatening situations increases alertness and arousal response to the conditions. On the other hand, over-activation of the limbic system that regulates wakefulness could cause hyper-arousal (22). Sleep disruption is frequently present with mental diseases, such as anxiety disorders, posttraumatic stress disorder, and depression. Elucidating the neural circuits that regulate physiological arousal in response to threats is essential for understanding maladaptive emotional states and stress-evoked sleep changes. We found that MePV^{Glu} neurons were activated by threat-evoked awakening from NREM sleep. Excitation of MePV^{Glu} neurons promoted wakefulness and increased anxiety-like behaviors. Different neural circuits of MePV^{Glu} neurons played different roles in regulating anxiety-like behaviors and sleep-wakefulness. MePV^{Glu} neurons promoted wakefulness through the MePV^{Glu}-PMCo and MePV^{Glu}-BNST pathways, but not through the MePV^{Glu}-VMH pathway. In contrast, MePV glutamatergic neurons promoted anxiety-like behaviors mainly through the MePV^{Glu}-VMH pathway. Our studies suggested that glutamatergic neurons in the MePV play a role in regulating anxiety-like behaviors and arousal responses to threatening stimuli. Over-activation of MePV glutamatergic neurons could cause hyperarousal response and obsessive anxiety-like behavior. Chemogenetic inhibition of MePV^{Glu} neurons produced an anxiolytic effect without affecting natural sleep-wake transitions.

After studying the neural circuits that control arousal for threat detection, we next explored the adaptive responses to chronic sleep deprivation. Chronic passive sleep deprivation increased anxiety-like behaviors and changed the structure of sleep, but the underlying mechanisms were barely known. We then explored the effect of chronic sleep deprivation on the activity of MePV neurons and downstream neuronal circuits using c-fos immunohistochemical staining and the fiber photometry. We found that 5 days of sleep deprivation activated the MePV^{Glu} neurons and increased MePV^{Glu} neurons-induced responses of PMCo and VMH glutamatergic neurons. However, MePV^{Glu} neurons-induced responses of BNST glutamatergic neurons were decreased by sleep deprivation. We next found that 1-day sleep deprivation significantly decreased wakefulness, and increased NREM sleep and REM sleep (Fig. 9C).

Because the mice were forced to stay awake during the sleep deprivation, the increased sleep after the sleep deprivation on Day 1 was reparative. But from the 2nd day on, the wakefulness increased and NREM sleep decreased (Fig. 9C), which suggested that the mice experienced a significant reduction in reparative sleep, and had a relative increase in total wakefulness and a relative decrease in NREM sleep duration. We next found that the inhibition of the MePV^{Glu} neurons reduced anxiety-like behaviors, decreased wakefulness and promoted NREM sleep after the sleep deprivation. The endogenous MePV^{Glu} neurons might inhibit restorative sleep after chronic sleep deprivation. These results indicated that MePV^{Glu} neurons could be potential targets for treating anxiety disorders and sleep disturbance. Though excitation of MePV^{Glu} neurons could decrease REM sleep in normal mice, inhibition of MePV^{Glu} neurons had no effect on REM sleep, no matter with or without the sleep deprivation. This phenomenon is due to the complexity and diversity of neural circuit functions. Further investigations should be made to explain it.

Studies have revealed lower alertness to the predator odour during REM sleep than in NREM sleep in rats (23). Previous studies have also demonstrated that the neuronal circuit comprising CRF neurons in the medial subthalamic nucleus (mSTN) regulated awakening from REM sleep by quickly integrating olfactory and visual signals (23). However, some other studies have revealed that acute optogenetic stimulation of GABA-BNST neurons—GABAergic neurons in the bed nucleus of the stria terminals—during NREM sleep causes an immediate transition to wakefulness. In contrast, stimulation during REM sleep has no impact on the sleep-wakefulness states in male mice (24). We speculate that regardless of whether the rapid awakening of animals depends on REM or NREM, it is closely related to the functions of different brain regions and circuits and the stimulus encountered by animals. In our experiments, sleep-wake transitions were evoked by the loud noise of opening the soundproofed door, which mimicked intrusion during sleeping. We found that MePV^{Glu} neurons were selectively active in noise-evoked awakening and from NREM sleep to REM sleep and changed little during natural NREM-to-wake transitions. Our data are consistent with previous experimental evidence that the human amygdala was activated during REM (25, 26). Some other studies have shown that REM is necessary for fear memory consolidation (27). Consistent with the result of *in vivo* calcium imaging recording, no effects were observed on sleep and wake time in the chemogenetic inhibition of endogenous MePV^{Glu} neurons. However, chemogenetic excitation of MePV^{Glu} neurons could promote wakefulness. These results suggested that endogenous MePV^{Glu} neurons might not affect wakefulness in normal states. MePV^{Glu} neurons only participated in responding to threats during sleep, and overexcited MePV^{Glu} neurons could lead to insomnia disorders. We also found that inhibiting the MePV^{Glu} neurons reduced anxiety-like behaviors, decreased wakefulness, and promoted NREM sleep after the 5 days of sleep deprivation. We supposed that there might be a threshold for these neurons to promote wakefulness. The activity of MePV^{Glu} neurons was below the threshold in the normal mice, and inhibiting these neurons did not cause changes in wakefulness. However, acute-threats or SD could increase neuronal activity exceeding the threshold range and thus promote wakefulness. Consistent with this inference, we found that the Ca^{2+} signal of MePV^{Glu} neurons was increased during NREM-wake transitions after 5 days of sleep deprivation (Supplementary Fig. 2F). This could also explain why chemogenetic inhibition of endogenous MePV^{Glu} neurons could promote NREM sleep after SD, but couldn't affect sleep in normal mice.

According to the results of the elevated plus maze test and open field test, chemogenetic excitation of MePV^{Glu} neurons enhanced anxiety-like behaviors, whereas chemogenetic inhibition of MePV^{Glu} neurons could alleviate anxiety-like behaviors. The results of fiber photometry during EPM showed high activity of MePV^{Glu} neurons when mice tried to explore the open arms, which reduced when mice entered

the closed arms. Similarly, a previous experiment showed an association between anxiety-like behaviors of rats and c-fos expression in MePV (13). Thus, we speculate that MePV^{Glu} neurons influence anxiety-related behaviors. Previous studies have shown that the PMCo might regulate male reproductive behavior, social odour, and primary olfactory processing (18, 24). The PMCo has feedback circuit connectivity with the accessory olfactory bulb and dense bilateral connectivity with the MeP (Me posterior) (18, 28). However, the functions of PMCo on wakefulness-sleep or anxiety are few. To identify the brain circuits that generate the MePV^{Glu}-PMCo pathway-mediated wakefulness, we measured cFos activity in the MePV^{Glu}-hM3Dq mice. Many cFos-positive cells were identified in multiple brain regions, especially in the PMCo. We thus investigated the function of the PMCo and found that the MePV^{Glu}→PMCo pathway was an important 'gate' for controlling wakefulness but not anxiety-like behaviors. Herein, we found that activation of the MePV^{Glu}→PMCo pathway increased the time spent on open arms in the elevated plus maze test and promoted locomotion in the open field test. Thus, stimulation of the MePV^{Glu} terminals in the PMCo could enhance motor ability. Our studies provided new evidence for the study of PMCo in sleep-wake research and provided groundbreaking direction for subsequent research.

Previous studies have suggested that regulation of anxiety-like behaviors requires the function of the BNST, whereas excitation of the BNST resulted in high anxiety-like behaviors (29, 30). Kim et al. identified that BNST coordinated the modulation of diverse anxiety features in which distinct subregions exert opposite effects in modulating anxiety (31). The BNST GABAergic system played a role in sleep–wakefulness control and reward-promoting CCK (cholecystokinin)-BNST neurons received their dense inputs from the Me, which provided an essential mechanism underlying the emotional arousal regulation and the pathophysiology of insomnia (24, 32, 33). We found that excitation of MePV^{Glu} neuronal terminals projecting to BNST promotes wakefulness. However, the MePV^{Glu}-BNST pathway did not participate in the regulation of anxiety-like behaviors. We also found that chronic sleep deprivation could decrease the responses of BNST glutamatergic neurons induced by optogenetic stimulation of MePV^{Glu} neurons. Therefore, the terminals of MePV^{Glu} neurons might regulate wakefulness mainly through controlling glutamatergic neurons of the BNST but not GABAergic neurons. Otherwise, more complicated micro-neuronal circuits in the BNST might also play a role in controlling GABAergic neurons. However, there is a need for further investigations to validate these findings.

The GABAergic neural circuits and astrocytes of VMH regulate anxiety and metabolism (34, 35). Several studies in related fields have indicated that the Me and the VMH are specific subregions involved in fear and anxiety caused by predator odor (36, 37). Our data on MePV^{Glu} -VMH are consistent with previous studies. In our experiments, excitation of MePV^{Glu} neuronal terminals projecting to VMH increased anxiety-like behaviors with no effect on sleep-wakefulness. It means that neural circuits of MePV^{Glu} -VMH may participate in mice anxiety caused by predator odour. There is a need for additional studies to investigate the mechanism underlying neural circuits.

The changes in wake time induced by optogenetic stimulation were more pronounced than changes in the second hour as seen in Figures 3E, 4E, and 5E. One explanation is that the stimulation might produce a short-term effect on arousal that could be quickly compensated by sleep pressure. Another possible reason is the fatigue of neurons after long-term excitation. Even if this hypothesis was true, the neuronal fatigue was short-term. During the experiment, we found that when these neurons were activated again the next day, they could still quickly promote arousal. Further investigations should be done on the impact of different durations of optogenetic stimulation on neuronal excitability. We will also conduct in-depth explorations of its mechanism in future work.

We found that the Ca^{2+} signal increased dramatically from NREM to REM sleep (Fig. 1E) but dropped

from REM to natural wake (Fig. 1F). These results suggested that MePV^{Glu} neurons might be active during REM sleep. Though activation of MePV^{Glu} neurons could decrease REM sleep (Fig. 2D and 3F), inhibition of MePV^{Glu} neurons didn't affect the NREM and REM sleep (Figure. 7). These inconsistent results illustrated the complexity of neuronal activity in nature. The mechanism by which MePV^{Glu} neurons regulate REM sleep might be as follows: There was a threshold for these neurons to promote the REM sleep transition. Below the threshold activity, although the transition to REM sleep might cause an increase in the activity of these neurons, it was only a concomitant activity and might not participate in determining the REM sleep transition. Therefore, inhibiting these neurons did not cause changes in the REM sleep. However, if these neurons were highly activated by the optogenetic stimulation, the increased neuronal activity exceeding the threshold range would cause a decrease in REM sleep. Another possible reason was that a reduction in NREM sleep mediated by optogenetic stimulation would also lead to a reduction in the transitions from NREM to REM

There might be different subclasses of MePV^{Glu} neurons responsible for different functions, because 5 days of sleep deprivation could lead to a decrease in NREM sleep, an increase in REM sleep, and an increase in anxiety-like behaviors. Inhibiting these neurons reduced anxiety-like behaviors and promoted NREM sleep, but did not affect the changes in REM sleep after sleep deprivation. These results suggested that the REM-related neurons might be a different subclass than those that regulate NREM sleep and anxiety-like behaviors. MePV^{Glu} neurons involved in REM sleep regulation might have other compensatory neural projections or even more complex neural circuit mechanisms, requiring further study. This also pointed out the direction for our subsequent research.

In summary, our findings suggest that the endogenous MePV^{Glu} neurons play a role in anxiety-related behaviors, but activation of MePV^{Glu} neurons could cause hyper-arousal response and obsessive anxiety-like behavior. Our study might provide critical underlying mechanisms for insomnia and anxiety disorders. In addition, this study provides a new perspective on treating anxiety disorders.

Materials and Methods

Sex as a biological variable

Male C57BL/6J wild-type mice were utilized for the experiments. Previous findings showed that the high hormone phase of proestrus in female mice increased wakefulness and decreased both NREM and REM sleep compared with other oestrous phases and in males (38).

Animals

All animal experiments were conducted in strict adherence to guidelines by the National Research Council on the Care and Use of Laboratory Animals. C57BL/6J (Beijing Vital River Laboratory Animal Technology Co., Ltd.) wild-type mice (male, weighing 25–30 g, and aged 8–12 weeks) were randomly chosen and utilized for the experiments. All mice were housed under a controlled environment, at a constant temperature of 22±2 °C, 50–60% humidity, and a 12 h/12 h light/dark cycle that began at zeitgeber time 0 (ZT 0). The animals were allowed unrestricted access to food and water. All behavioral tests were performed during the light cycle between 9: 00 h and 17: 00 h. Both the number of mice utilized and suffering were kept to a minimum. All experimental procedures were approved by the Institute of Animal Care Committee at Wuhan University's Zhongnan Hospital.

Virus injection

The projection targets were set as follows: MePV: AP: -1.58 mm, ML: 2.02 mm, DV: -5.50 mm; BNST: AP = -0.25mm, ML = ±0.75mm, DV = -3.80 mm; VMH: AP = -1.45mm, ML = ±0.55 mm, DV = -5.60 mm; PMCo: AP = -2.80 mm, ML = ±2.95 mm, DV = -5.50 mm. The virus was injected using a micropipette with a 20 m aperture, fitted with the Auto-Nanoliter Injector (Harvard) at a rate of 10 nl/min. After microinjection, the micropipette was placed and held for 10 minutes to ensure vector diffusion, and then gently removed. Detailed information was provided in Supplemental Experimental Procedures.

EEG-EMG recordings and analysis

Detailed information was provided in Supplemental Experimental Procedures.

Fiber photometry

Preoperative preparations for implantation of the optic fibers were performed as described above, two weeks following virus injection. The mice were implanted with optical fibers with a 200 m diameter and a numerical aperture (NA) of 0.37 (Inper Tech, China). Briefly, the fiber was first carefully dropped over the MePV (bregma coordinates: AP = 1.58 mm; ML = +2.02 mm; DV = -5.35 mm). Other fiber positions were set as follows: BNST: AP = -0.25mm, ML = ±0.75mm, DV = -3.80 mm; VMH: AP = -1.45mm, ML = ±0.55 mm, DV = -5.60 mm; PMCo: AP = -2.80 mm, ML = ±2.95 mm, DV = -5.50 mm. Then the mice were implanted with electroencephalogram (EEG) electrodes as described above. Next, the fiber was attached to the surface of the skull using a small coating of Super-Bond C&B dental cement, and then the second coat of regular dental cement was used to securely bind the fiber. The mice were kept separately after surgery to ensure proper recovery.

For fiber photometry tests, detailed information was provided in Supplemental Experimental Procedures. We primarily recorded the Ca^{2+} dynamics at two event-related time intervals during the EPM tests for the Ca^{2+} signal analysis: (A) when the mice reached the open arms and (B) when they made their way back to the closed arms. We also captured the Ca^{2+} signal 10 seconds before and 10 seconds after the events.

We primarily recorded Ca^{2+} dynamics at six event-related periods during the wake-sleep experiments as follows: (A) NREM-threat-evoked awakening; (B) NREM - REM; (C) REM - natural wake; (D) NREM - natural wake; (E) REM - microarousal - NREM; and (F) NREM - microarousal - NREM. The Ca^{2+} signal was captured 30 seconds before until 30 seconds after the events. Fr threat-evoked awakening, sleep-wake transitions were elicited by the jarring sound opening the soundproofed door to the recording chamber, which mimicked an intruder's stimulus while the mice were asleep.

Fiber ferrule implantation

Implantation of the Fiber ferrule was performed two weeks after virus injection using the procedure described above. Summarily, mice were implanted with an optical fiber ferrule (diameter: 200 m, NA: 0.37, Inper Tech, China) above the MePV glutamatergic neurons for optical stimulation (same coordinates as fiber photometry). To stimulate MePV output projections, fiber ferrules were implanted into the ventromedial hypothalamic nucleus, bed nucleus of the stria terminals, and posteromedial cortical amygdaloid area. Fiber positions were set as follows: the MePV: AP = 1.58 mm; ML = +2.02 mm; DV = -5.0 mm; BNST: AP = -0.25mm, ML = ±0.75mm, DV = -3.30 mm; VMH: AP = -1.45mm, ML = ±0.55 mm, DV = -5.10 mm; PMCo: AP = -2.80 mm, ML = ±2.95 mm, DV = -5.0 mm.

Optical stimulation

Mice were hooked up to optical cables, five days after implantation of EEG-EMG electrodes, then allowed at least two days to acclimatize to the recording box. A waveform generator was used to control lasers that emit blue light at 473 nm (Thinker Tech, China). Next, a 473 nm laser's output power at the fiber's tip was measured between 5-8 mW using an optical power meter (PM100D, Thorlabs, United States). During NREM or REM sleep, random pulses of 473 nm light of 10 ms width at 5 to 20 Hz were administered to optogenetically excite MePV glutamatergic neurons and MePV projections. The EEG-EMG signal was visually monitored in real-time, and optical stimulation was applied after the onset of stable NREM sleep (~5 min from onset) until awake or until 60 s. If the mouse did not wake up within 60 s, the latency period is defined as 60s. We used the sleeping posture (curl up still and eyes closed) and the EEG-EMG of the mouse to determine whether the mouse had entered sleep. If the mouse did not wake up within 60 s, the latency period is defined as 60s. We used the sleeping posture (curl up still and eyes closed) and the EEG-EMG of the mouse to determine whether the mouse had entered sleep. The NREM-REM transitions occurred during sleep. About 5min after the mouse entered sleep, the new onset of NREM sleep was chosen and the optical stimulus was delivered. For extended stimulation, from ZT 2 to ZT 4, 4 s in every minute of 10 ms width pulses at 10 Hz were used. Blue light stimulation (wavelength: 470 nm; frequency: 10 Hz; width: 10 ms; power: 5-8 mW) was administered through the optical cannula during the experimental stage of the elevated plus maze or open field test. All optogenetic experiments were performed between ZT 2 and ZT 10.

Elevated plus maze (EPM)

Mice were allowed to acclimatize to the testing space for 30 minutes and then put on the raised plus maze. The elevated plus maze comprised 3 sections as follows: two opposed closed arms (50 x 10 cm each) with 40 cm tall opaque walls, two opposite open arms (50 x 10 cm each), and a middle section (10 x 10 cm). Additionally, the experimental equipment was raised 50 centimeters above the ground. The animals were initially positioned in the labyrinth facing the closed arm, and then the time spent on open and closed arms was recorded over a 5-min period. After the trial, the experimental box was cleaned of mouse waste and treated with ethanol cotton to get rid of the scent of the preceding mouse. Less exploration on open arms is linked to anxiety-related behaviors (39, 40).

Open field test (OFT)

Mice were given at least 30 minutes to get used to the testing room, positioned in the corner of the opening experimental box (50 cm, 50 cm, 40 cm) and watched for five minutes. Average movement speeds (mm/s) and total lengths traveled (m) throughout the center period were measured. After the trial, the experiment box was cleaned of mouse waste and treated with cotton soaked in ethanol to remove the scent of the preceding mouse. Less center-area exploration is linked to anxiety-related behaviors.

Electrophysiological analysis

The patch clamp recording was performed as previously described (41, 42). Detailed information was provided in Supplemental Experimental Procedures.

Histology

Immunohistochemistry was performed as described previously (43, 44). Detailed information was provided in Supplemental Experimental Procedures.

Sleep deprivation:

Sleep deprivation was achieved from day 1 to day 5 using an automated sleep deprivation system as described previously (45, 46) Detailed information was provided in Supplemental Experimental Procedures.

Data analysis

Data were presented as means ± standard error of the mean (SEM). Sample sizes were calculated based on past publications using optogenetic and chemogenetic approaches to investigate the sleep-wake circuitry (43, 44). The normality of each dataset was initially assessed using the Shapiro-Wilk test, and those that conformed to a normal distribution were subjected to parametric analyses. We used paired or unpaired two-taile t-tests to compare the means between the two groups. Non-normally distributed datasets were analyzed using the Mann-Whitney rank sum or the Wilcoxon signed-rank tests. Comparisons across 3 or more groups were performed using one-way ANOVA test or two-way ANOVA test, followed by Sidak's post hoc test. All statistical analyses were performed using SPSS 26.0, GraphPad Prism 9.0, or Matlab R2018a where necessary. Statistical significance was set at $P < 0.05$.

Study approval

All experiments were approved by the Institute of Animal Care Committee at Wuhan University's Zhongnan Hospital in Wuhan, Hubei Province, China.

Data and materials availability

All data needed to evaluate the conclusions in the paper are present in the paper and/or the Supplementary Materials. Values for all data points shown in graphs and behind any reported means are available in the Supporting Data Values.

Author Contributons

Conceptualization, H.B.X., L.L.B., P.C., and Y.L.; Methodology, Y.C.D., Y.L., and Y.F.Z.; Investigation, Y.C.D., Y.L., Y.F.Z., Y.D.L., M.C., Y.X.W.,J.Y.Z.,L.K.W, and Y.F.C.; Writing – Original Draft, Y.L. and L.L.B.; Writing Review & Editing, H.B.X., L.L.B., and P.C.; Funding Acquisition, H.B.X. and L.L.B.; Resources, H.B.X. and L.L.B.; Supervision, H.B.X., L.L.B. and P.C.

Acknowledgements and Funding

We appreciated Tian-ming Gao for his helpful advice and technological support. This work received financial support from the National Natural Science Foundation of China (under Grant Nos 81771819 and 32071140), the National Key Research and Development Plan of China (Project 2017YFC0108803), the funds for the Hubei Province Natural Science Foundation (2020CFB593) and the key project of the Hubei Provincial Health and Health Committee Joint Fund (Project WJ 2019H058), the National Natural Science Foundation of China and the Swedish International Cooperation Fund for Research and Education (NO. 8201101416), the Scientific Research Project of Traditional Chinese Medicine of Hubei Province (ZY2023Q032) and Research Grant of Guangdong Province Key Laboratory of Psychiatric

Disorders(N202301).

Declaration of interests

The authors declare no competing interests.

References:

1. Junhong Y, Iris R, Johnson F, Min-Jun J, Lei F, Heok KE, et al. Sleep correlates of depression and anxiety in an elderly Asian population. *Psychogeriatrics : the official journal of the Japanese Psychogeriatric Society.* 2016;16(3).
2. Scarpa JR, Jiang P, Gao VD, Fitzpatrick K, Millstein J, Olker C, et al. Cross-species systems analysis identifies gene networks differentially altered by sleep loss and depression. *Science Advances.* 2018;4(7).
3. A KD, R AJ, and L DC. The impact of stress on sleep: Pathogenic sleep reactivity as a vulnerability to insomnia and circadian disorders. *Journal of sleep research.* 2018;27(6).
4. G FR. Sleep, circadian rhythms and health. *Interface focus.* 2020;10(3).
5. Lang PJ, and McTeague LM. The anxiety disorder spectrum: Fear imagery, physiological reactivity, and differential diagnosis*. *Anxiety, Stress & Coping.* 2009;22(1):5-25.
6. Jansson-Fröjmark M, and Lindblom K. A bidirectional relationship between anxiety and depression, and insomnia? A prospective study in the general population. *Journal of Psychosomatic Research.* 2008;64(4):443-9.
7. T GC, and Sabino CN. The many paths to fear. *Nature reviews Neuroscience.* 2012;13(9).
8. Ann K, S. KP, yun LL, Stefanos S, A. WD, and J. AD. Stimulus-specific hypothalamic encoding of a persistent defensive state. *Nature.* 2020;586(7831).
9. Bian X. Physiological and morphological characterization of GABAergic neurons in the medial amygdala. *Brain Research.* 2013;1509.
10. Niimi K, Horie S, Yokosuka M, Kawakami-Mori F, Tanaka K, Fukayama H, et al. Heterogeneous electrophysiological and morphological properties of neurons in the mouse medial amygdala in vitro. *Brain Research.* 2012;1480.
11. Bian X, Yanagawa Y, Chen WR, and Luo M. Cortical-Like Functional Organization of the Pheromone-Processing Circuits in the Medial Amygdala. *Journal of Neurophysiology.* 2008;99(1):77-86.
12. Choi GB, Dong H-w, Murphy AJ, Valenzuela DM, Yancopoulos GD, Swanson LW, et al. Lhx6 Delineates a Pathway Mediating Innate Reproductive Behaviors from the Amygdala to the Hypothalamus. *Neuron.* 2005;46:647-60.
13. Vanderhaven MW, Cornish JL, and Staples LG. The orexin-1 receptor antagonist SB-334867 decreases anxiety-like behavior and c-Fos expression in the hypothalamus of rats exposed to cat odor. *Behavioural Brain Research.* 2015;278.
14. Dielenberg RA, Hunt GE, and McGregor IS. ‘When a rat smells a cat’: the distribution of Fos immunoreactivity in rat brain following exposure to a predatory odor. *Neuroscience.*

2001;104(4):1085-97.
15. Miller SM, Marcotulli D, Shen A, and Zweifel LS. Divergent medial amygdala projections regulate approach–avoidance conflict behavior. *Nature Neuroscience.* 2019;22(4):565-75.
16. Cheung CC, Krause WC, Edwards RH, Yang CF, Shah NM, Hnasko TS, et al. Sex-dependent changes in metabolism and behavior, as well as reduced anxiety after eliminating ventromedial hypothalamus excitatory output. *Molecular Metabolism.* 2015;4(11).
17. Jose R-R, L. UR, Hiroshi N, M. OJ, L. BM, M.K. NV, et al. Prepronociceptin-Expressing Neurons in the Extended Amygdala Encode and Promote Rapid Arousal Responses to Motivationally Salient Stimuli. *Cell Reports.* 2020;33(6).
18. Livio O, Eleonora R, Tuyen T, Daniel D, and G CJ. Amygdala Corticofugal Input Shapes Mitral Cell Responses in the Accessory Olfactory Bulb. *eNeuro.* 2018;5(3).
19. Renouard L, Billwiller F, Ogawa K, Clément O, Camargo N, Abdelkarim M, et al. The supramammillary nucleus and the claustrum activate the cortex during REM sleep. *Science Advances.* 2015;1(3).
20. J SV, Matthew C, Romain D, Joseph D, W FM, Hannah L, et al. Cortical-subcortical structural connections support transcranial magnetic stimulation engagement of the amygdala. *Science advances.* 2022;8(25).
21. Ying L, Bo R, Shuang L, Ning Z, Jie W, Linlin B, et al. Distinct Hypothalamic Paraventricular Nucleus Inputs to the Cingulate Cortex and Paraventricular Thalamic Nucleus Modulate Anxiety and Arousal. *Frontiers in Pharmacology.* 2022;13.
22. Sleep disturbances in veterans with chronic war-induced PTSD. *Journal of Injury and Violence Research.* 2016;8(2).
23. YuTing T, Binghao Z, Shanping C, Jialin Y, Jingjing L, Lisha L, et al. The subthalamic corticotropin-releasing hormone neurons mediate adaptive REM-sleep responses to threat. *Neuron.* 2022;110(7).
24. Shota K, Shingo S, and Takeshi S. Excitation of GABAergic Neurons in the Bed Nucleus of the Stria Terminalis Triggers Immediate Transition from Non-Rapid Eye Movement Sleep to Wakefulness in Mice. *The Journal of neuroscience : the official journal of the Society for Neuroscience.* 2017;37(30).
25. María C-C, Francisco V, Yolanda DR-P, L AJ, David T-M, A GM, et al. Human amygdala activation during rapid eye movements of rapid eye movement sleep: an intracranial study. *Journal of sleep research.* 2016;25(5).
26. L. WL, Gyorgy L, M. AA, and D. SL. Regulation of dark period sleep by the Amygdala: A microinjection and optogenetics study. *Brain Research.* 2022;1781(prepublish).
27. Menz MM, Rihm JS, Salari N, Born J, Kalisch R, Pape HC, et al. The role of sleep and sleep deprivation in consolidating fear memories. *NeuroImage.* 2013;75.
28. DiBenedictis BT, Helfand AI, Baum MJ, and Cherry JA. A quantitative comparison of the efferent projections of the anterior and posterior subdivisions of the medial amygdala in female mice. *Brain Research.* 2014;1543.
29. Kalin NH, Shelton SE, Fox AS, Oakes TR, and Davidson RJ. Brain Regions Associated with the Expression and Contextual Regulation of Anxiety in Primates. *Biological Psychiatry.* 2005;58(10):796-804.
30. Sullivan GM, Apergis J, Bush DEA, Johnson LR, Hou M, and Ledoux JE. Lesions in the bed nucleus of the stria terminalis disrupt corticosterone and freezing responses elicited by a

contextual but not by a specific cue-conditioned fear stimulus. *Neuroscience.* 2004;128(1):7-14.

31. Sung-Yon K, Avishek A, Yeun LS, H MJ, K KC, S MC, et al. Diverging neural pathways assemble a behavioural state from separable features in anxiety. *Nature.* 2013;496(7444).
32. J GW, Ada E-R, J CD, Shi-Bin L, C MR, and Luis dL. Parallel circuits from the bed nuclei of stria terminalis to the lateral hypothalamus drive opposing emotional states. *Nature neuroscience.* 2018;21(8).
33. J. GW, and B. PM. Extended Amygdala Neuropeptide Circuitry of Emotional Arousal: Waking Up on the Wrong Side of the Bed Nuclei of Stria Terminalis&#13. *Frontiers in Behavioral Neuroscience.* 2021;15.
34. Yang F, Liu Y, Chen S, Dai Z, Yang D, Gao D, et al. A GABAergic neural circuit in the ventromedial hypothalamus mediates chronic stress–induced bone loss. *Journal of Clinical Investigation.* 2020;130(12):6539-54.
35. Yunhui L, Jie S, Dashuang G, Lu Z, and Fan Y. Astrocytes in the Ventromedial Hypothalamus Involve Chronic Stress-Induced Anxiety and Bone Loss in Mice. *Neural Plasticity.* 2021;2021.
36. Pérez-Gómez A, Bleymehl K, Stein B, Pyrski M, Birnbaumer L, Munger SD, et al. Innate Predator Odor Aversion Driven by Parallel Olfactory Subsystems that Converge in the Ventromedial Hypothalamus. *Current Biology.* 2015;25(10).
37. Rosen JB, eAsok A, and eChakraborty T. The smell of fear: innate threat of 2,5-dihydro-2,4,5-trimethylthiazoline, a single molecule component of a predator odor. *Frontiers in Neuroscience.* 2015;9.
38. Swift KM, Keus KM, Echeverria CG, Cabrera Y, Jimenez J, Holloway JK, et al. Sex differences within sleep in gonadally-intact rats. *Sleep.* 2019.
39. Gao F, Huang J, Huang G-B, You Q-L, Yao S, Zhao S-T, et al. Elevated prelimbic cortex-to-basolateral amygdala circuit activity mediates comorbid anxiety-like behaviors associated with chronic pain. *Journal of Clinical Investigation.* 2023;133(9).
40. YiHua C, JianLin W, NengYuan H, JiaPai Z, WeiPeng L, ShengRong Z, et al. Distinct projections from the infralimbic cortex exert opposing effects in modulating anxiety and fear. *The Journal of clinical investigation.* 2021;131(14).
41. Wang X, Liu D, Huang H-Z, Wang Z-H, Hou T-Y, Yang X, et al. A Novel MicroRNA-124/PTPN1 Signal Pathway Mediates Synaptic and Memory Deficits in Alzheimer's Disease. *Biological Psychiatry.* 2018;83(5).
42. Ming C, and Lin-Lin B. Optogenetic Long-Term Depression Induction in the PVT-CeL Circuitry Mediates Decreased Fear Memory. *Molecular neurobiology.* 2019;56(7).
43. Ren S, Wang Y, Yue F, Cheng X, Dang R, Qiao Q, et al. The paraventricular thalamus is a critical thalamic area for wakefulness. *Science.* 2018;362(6413).
44. Yu X, Li W, Ma Y, Tossell K, Harris JJ, Harding EC, et al. GABA and glutamate neurons in the VTA regulate sleep and wakefulness. *Nature Neuroscience.* 2019;22(1).
45. WenJie B, L BC, A KJ, and Luis dL. Adolescent sleep shapes social novelty preference in mice. *Nature neuroscience.* 2022;25(7).
46. K YR, R LM, ManuelMiguel R, E NM, S TA, S UD, et al. Differential effect of sleep deprivation on place cell representations, sleep architecture, and memory in young and old mice. *Cell reports.* 2021;35(11).

Fig. 1

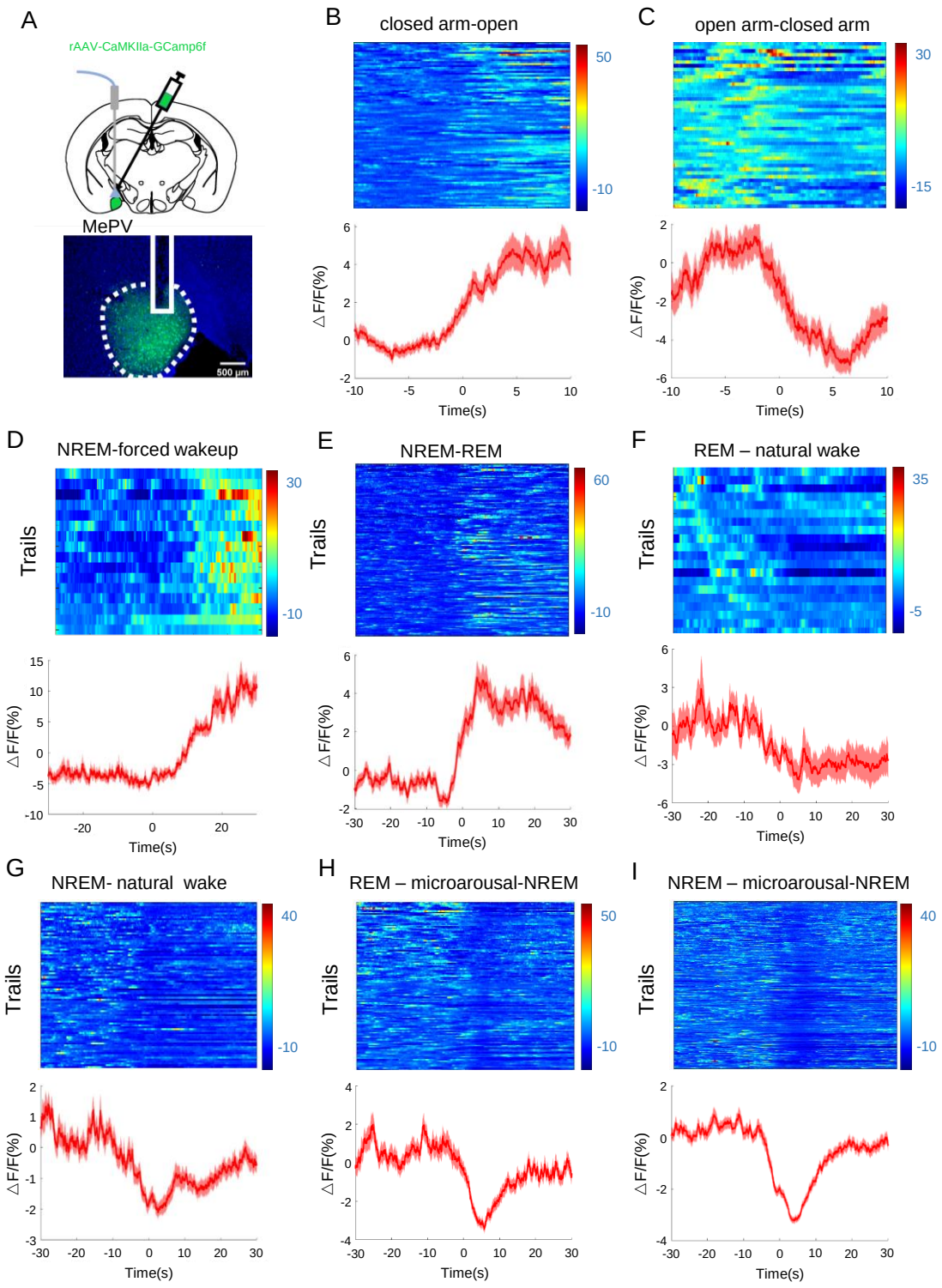

Fig. 1. The effects of NREM-to-REM transitions, NREM-to-unusual wake transitions, and REM-to-wake transitions on the activity of MePV glutamatergic neurons. A, Top: The *in vivo* recording

arrangement; Down: Illustrations of the MePV from a mouse expressing the rAAV-CaMKIIa-GCaMP6f virus (n = 6 mice/group), displaying virus expression as well as the position of the fiber tip above the MePV. **B,** The heat map for the calcium signal of MePV glutamatergic neurons. The representative transitions (closed arm-open arm, 87 trials) of the changes in color-coded fluorescence intensity. **C,** The color-coded fluorescence intensity changes of the representative shifts from the open arm to the closed arm (45 trials). **D,** A shift in color-coded fluorescence intensity illustrating the representative transition from NREM to forced wakeup (16 trials). **E,** Changes in color-coded fluorescence intensity indicating the representative transitions from NREM to REM (132 trials). **F,** The representative shifts in fluorescence intensity during the transitions from REM to normal wakefulness (20 trials). **G,** Representative shift in color-coded fluorescence intensity (83 trials) depicting the transition from NREM to natural wake. **H,** Color- changes representing shifts in fluorescence intensity from REM to microarousal (119 trials). **I,** A shift in the intensity of the color-coded fluorescence indicating the representative transition from NREM to microarousal (257 trials). Mean (red trace) ± SEM (red shading) represents the average responses of all the transitions.

Fig. 2

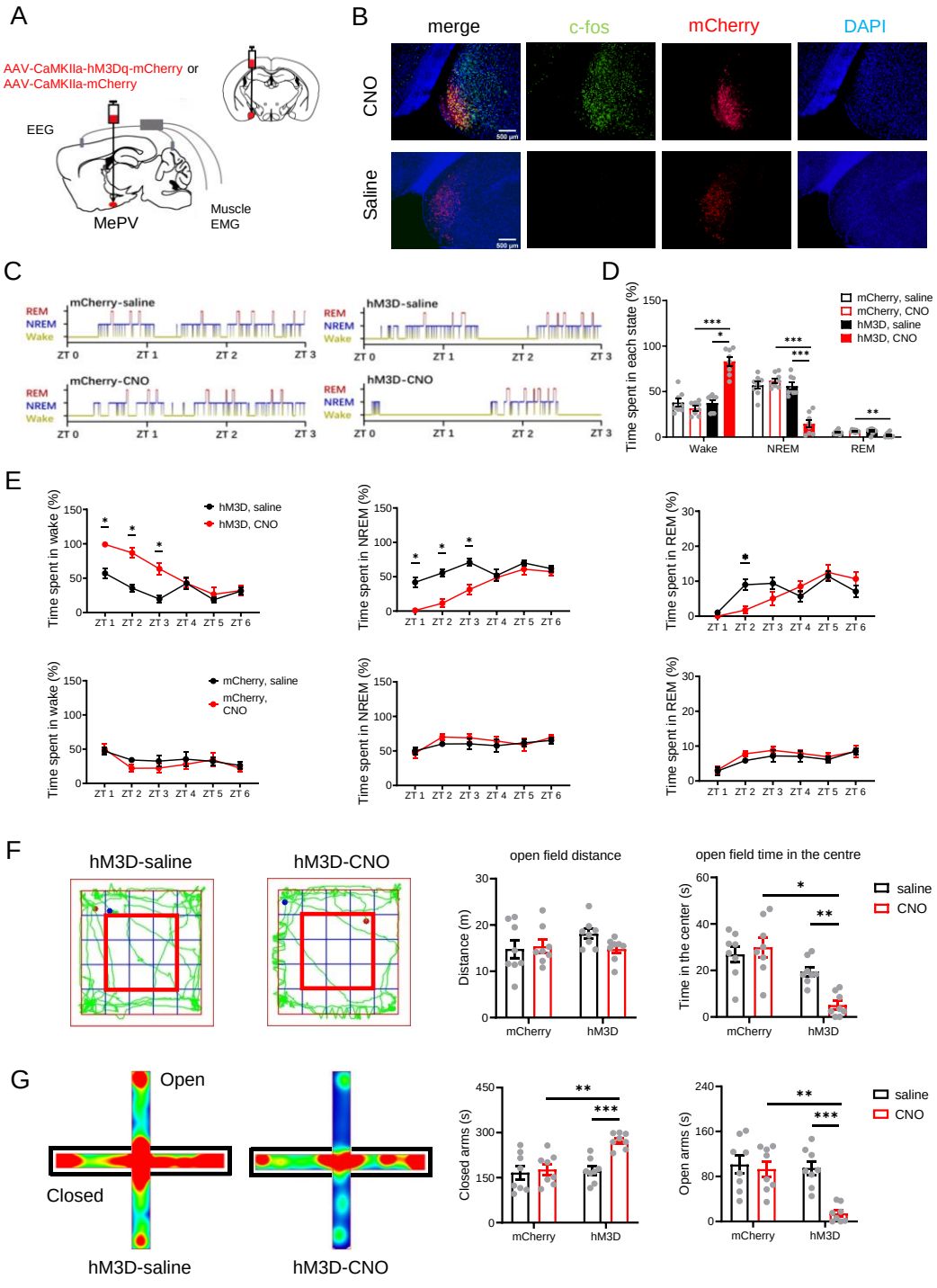

Fig. 2. The effects of chemogenetic excitation of MePV^{Glu} neurons on wakefulness and anxiety-like behavior. A, Schematic diagram showing AAV-CaMKIIa-hM3Dq-mCherry/AAV-CaMKIIa-mCherry virus injection and EEG-EMG recordings. **B,** Representative images (10x) of c-fos (green), mCherry (red), and DAPI (blue) colocalization in MePV^{Glu} neurons of MePV^{Glu}-hM3Dq-mCherry mice

treated with CNO or saline. Scale bar =500 µm. **C,** 3-hour hypnograms following saline or CNO (1 mg/kg) injections into a MePV^{Glu}- mCherry mouse (left) and a MePV^{Glu}-hM3Dq-mCherry mouse (right). **D,** Percentages of time spent in each state for MePV^{Glu}-hM3Dq-mCherry mice and MePV^{Glu}-mCherry mice 3 hours after CNO injection. **E,** Time spent in each condition 6 hours after injection of saline or CNO (1 mg/kg) into the MePV^{Glu}-hM3Dq-mCherry mice (top) and the MePV^{Glu}-mCherry mice (bottom). **F,** left panel: Representative track plots of MePV^{Glu}-hM3Dq-mCherry mouse treated with saline and CNO in open field test (red frame represents the central zone). Right panel: Time spent in the center zone and distance traveled of MePV^{Glu}-hM3Dq-mCherry mice and MePV^{Glu}-mCherry mice. **G,** left panel: Representative heatmaps of MePV^{Glu}-hM3Dq-mCherry mouse treated with saline and CNO in elevated plus maze (Closed arms on black frames). Right panel: Time spent in open/closed arms of MePV^{Glu}-hM3Dq-mCherry mice and MePV^{Glu}-mCherry mice. Wilcoxon signed rank test or two-way RM ANOVA test with Sidak's post hoc comparison for **D**-**E**. Two-way RM ANOVA test with Sidak's post hoc for **F**-**G**. N = 8 per group. *P < 0.05, **P < 0.01, ***P < 0.001.

Fig. 3

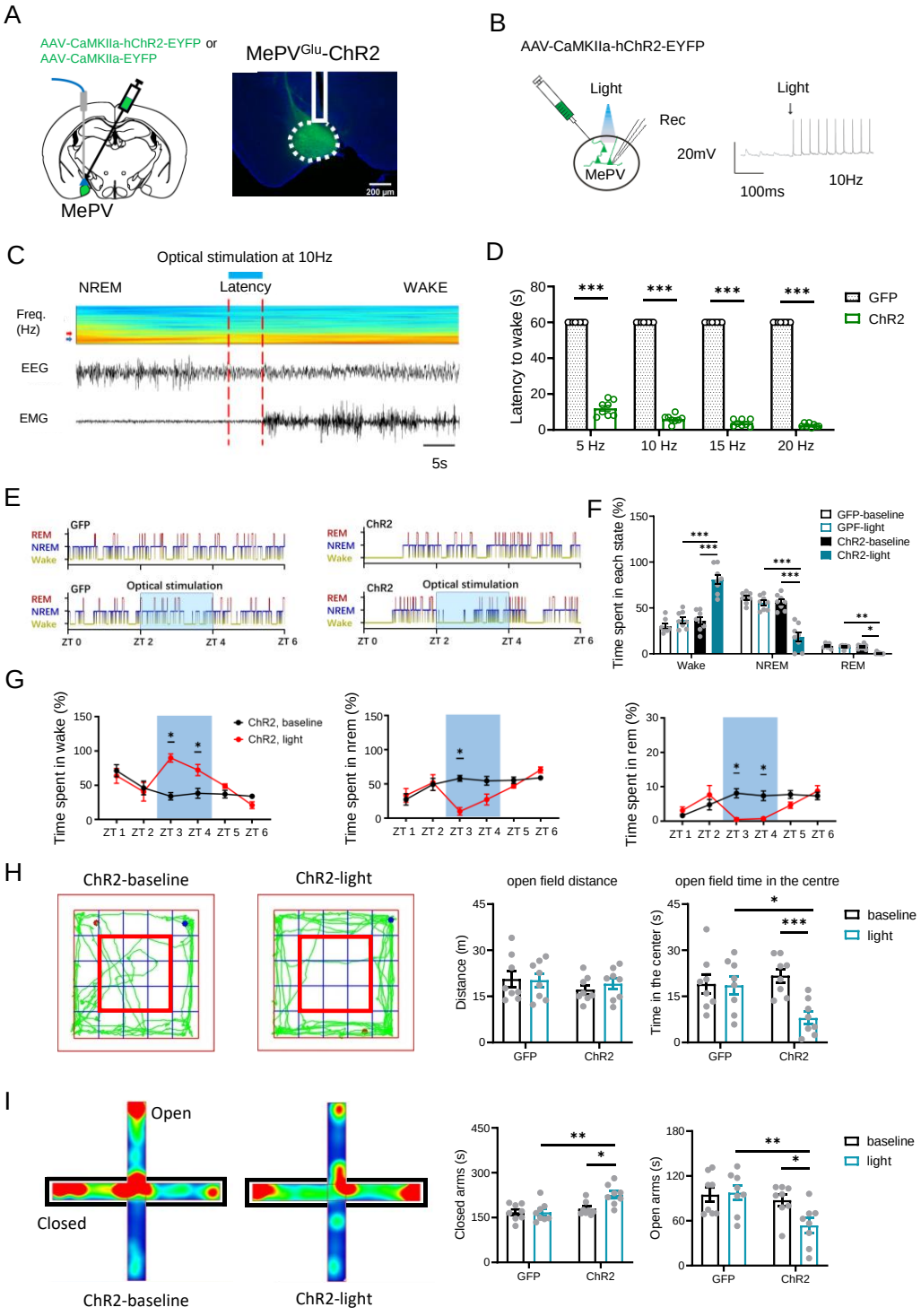

Fig. 3. The effects of optogenetic stimulation of MePV glutamatergic neurons on wakefulness and anxiety-like behavior. A, Schematic of AAV-CaMKIIa-hChR2-GFP/AAV-CaMKIIa-GFP virus injection and optogenetic modulation of MePV^{Glu} neurons (left panel). AAV-CaMKIIa-ChR2-GFP expression and optical fiber placement in the MePV (right panel). Scale bar =200 μm. **B,**

Electrophysiology recordings of MePV^{Glu} neurons expressing ChR2 triggered by blue light pulses at 10Hz. **C,** An EEG spectrogram and EEG-EMG trace showed that 10-Hz stimulation was administered during NREM sleep. The arrowheads represent 4 and 8 Hz. The color scale represents the raw power spectral density (mV2). **D,** Latencies to awaken from sleep in response to varied frequencies of visual stimulation (one stimulation/animal). The latencies of NREM to wake were gradually reduced by the higher light stimulation at frequencies of 5Hz, 10Hz, 15Hz, and 20Hz, respectively. **E,** Hypnograms for Sleep and wakefulness. The optical stimulation of 2 hours was performed in the ChR2 group (470nm, 10Hz, 4s /60s, 2h). **F,** The time spent in each state during two hours of light stimulation. **G,** The wakefulness, NREM, and REM sleep duration of MePV^{Glu}-ChR2 mice subjected to 2 hours of opto-stimulation (10 Hz for 4 seconds with a 56-second interval). **H,** Open field test track plots with representative track plots (left). Time spent in the center zone and distance traveled (right). The red frame represents the central zone. **I,** Heatmaps depiction of raised plus maze testing (left) and time spent on open/closed arms (right). Mann-Whitney rank sum test for **D**. Wilcoxon signed rank test, Mann-Whitney rank sum test or two-way RM ANOVA with Sidak's post hoc comparison for **F**. Wilcoxon signed rank test for **G** and **I**. Two-way RM ANOVA with Sidak's post hoc comparison for **H**. N= 8 per group. All error bars are SEM. *P < 0.05, **P < 0.01, and ***P < 0.001

Fig. 4

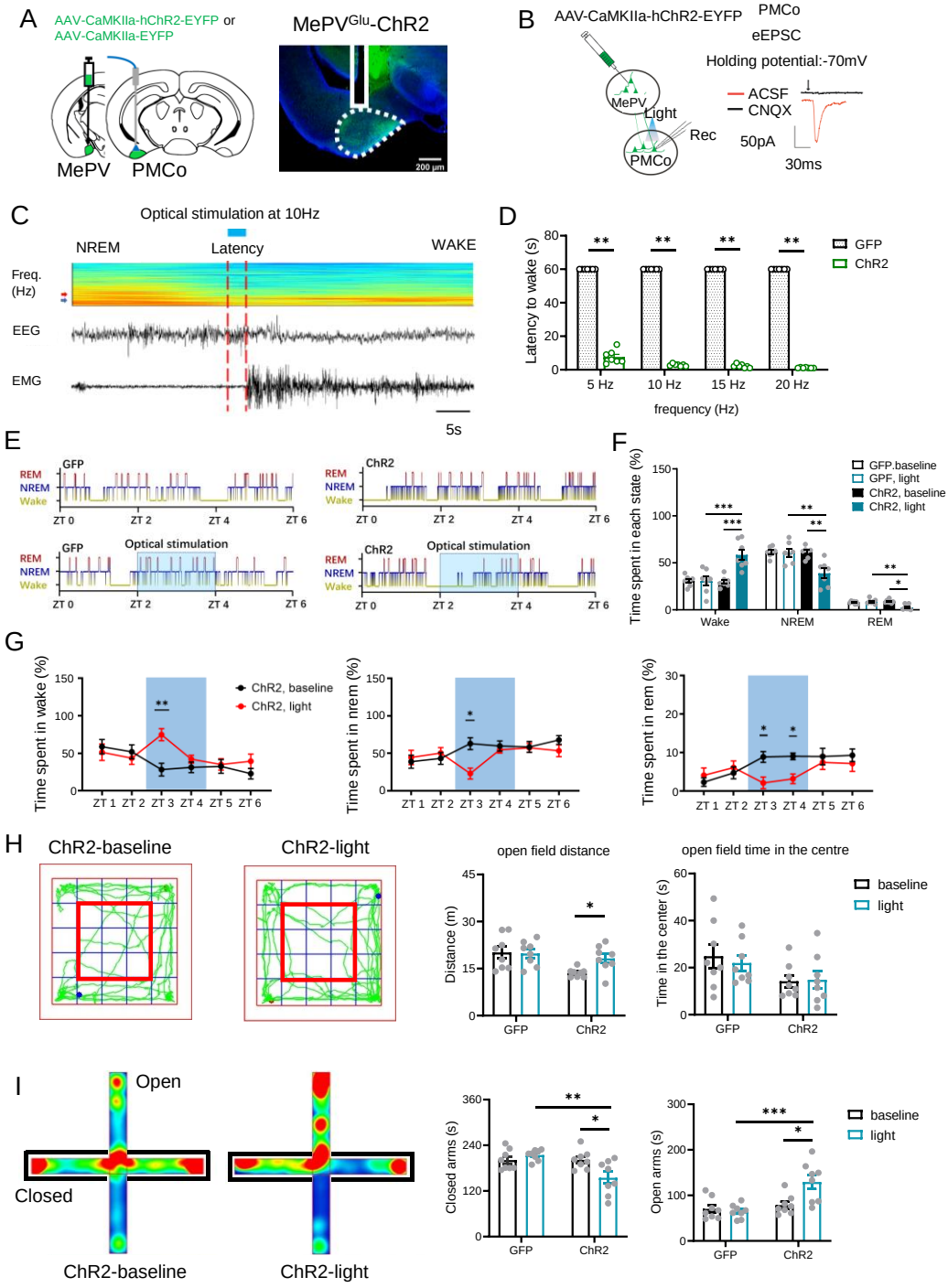

Fig. 4. The regulation of wakefulness and anxiety-like behaviors by MePV^{Glu}-PMCo circuit. A, An optical fiber was implanted into the PMCo region of MePV^{Glu}-ChR2 mice (left panel). The distribution of ChR2-expressing MePV glutamatergic terminals and the position of optical fiber in the PMCo(Right panel). Scale bar =200 μm. **B,** Patch-clamp electrophysiology diagram (left panel). The evoked EPSC

was induced by 2 Hz laser stimulation in the PMCo (right panel). **C,** Representative EEG spectrogram and EEG-EMG recordings. During NREM sleep, 10 Hz light stimulation was administered (Red arrow: 4 Hz; Blue arrow: 8 Hz; Freq., frequency). The color scale represents the raw power spectral density (mV2). **D,** Latencies to awaken from sleep following varied frequencies of light stimulation (once per animal, n = 7 per group). **E,** A 2 h light stimulation hypnograms during the light phase. **F,** Time spent in each state throughout 2 hours of optogenetic stimulation (n = 7 per group). **G,** The waking time, NREM time, and REM time of MePV^{Glu}-PMCo ChR2 mice subjected to 2 hours of opto-stimulation (10 Hz for 4 seconds with 56-second intervals). **H,** Representative track plots (left). The time spent in the center zone and distance traveled (right) in the open field test. The red frame represents the middle zone (n = 8 per group). **I,** EPM's heatmap representation (on the left), and time spent on open/closed arms (right) (n = 8 per group). Mann-Whitney rank sum test for **D**. Wilcoxon signed rank test, Mann-Whitney rank sum test or two-way RM ANOVA with Sidak's post hoc comparison for **F**. Wilcoxon signed rank test, Mann-Whitney rank sum test or paired t test for **G**. Two-way RM ANOVA with Sidak's post hoc comparison where applicable for **H** and **I**. *P < 0.05, **P < 0.01, ***P < 0.001

Fig. 5

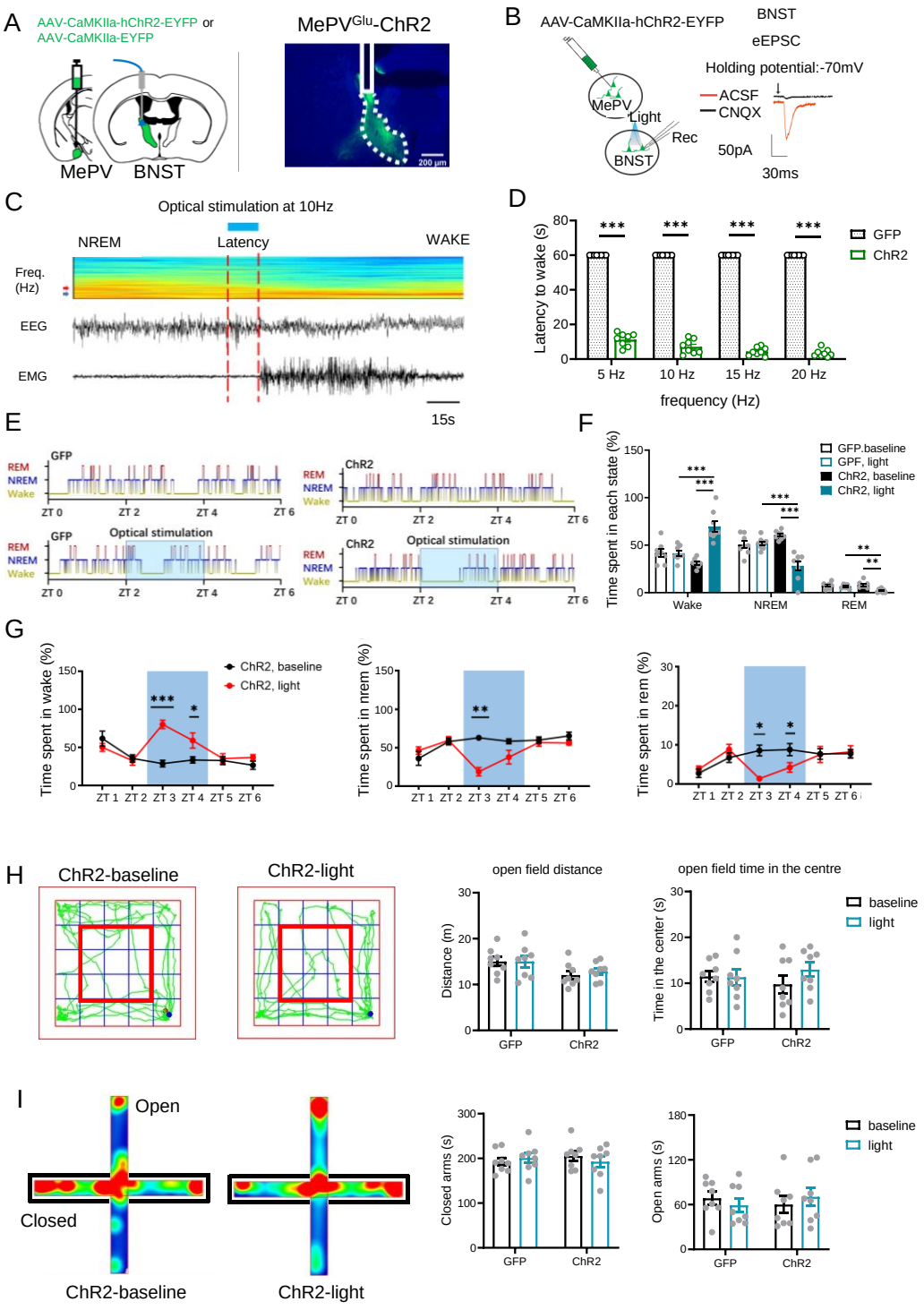

Fig. 5. The effects of the MePV^{Glu}-BNST pathway on wakefulness and anxiety-like behaviors. A, An optical fiber was implanted into the BNST region of MePV^{Glu}-ChR2 mice to investigate the function of MePV^{Glu}-BNST projection (left). The picture depicted the distribution of ChR2-expressing MePV glutamatergic terminals in the BNST as well as the placement of optical fiber (right). Scale bar

=200 μm. **B,** Patch-clamp electrophysiology diagram (left). In the BNST, voltage-clamp traces revealed the EPSC induced by 2 Hz laser stimulation (right). **C,** EEG spectrogram and EEG-EMG trace showed that 10-Hz stimulation was administered during NREM sleep (Red arrow: 4 Hz; Blue arrow and 8 Hz). The color scale represents the raw power spectral density. The latencies of NREM-to-wake were shortened by the high stimulation frequencies. **D,** Latencies to awaken from sleep following varied frequencies of optical stimulation (once/animal; GFP: 8 mice; ChR2: 8 mice). **E,** The optical stimulation hypnograms during the light phase (470nm, 10hz, 4s /60s, 2h). **F,** Time spent in each state throughout 2 hours of light stimulation. **G,** MePV^{Glu}-BNST-ChR2 mice were subjected to 2 hours of opto-stimulation (10 Hz for 4 seconds with a 56-second interval), and the proportions of waking, NREM, and REM sleep duration were recorded. **H,** Track plots for open field test (left). The open field test included time spent in the center zone and distance traveled (right). The red frame represents the central zone. **I,** Heatmaps of the elevated plus maze test (left) and the time spent on the open/closed arms (right). Mann-Whitney rank sum test for **D**. Wilcoxon signed rank test, Two-way RM ANOVA with Sidak's post hoc comparison for **F**, G, **H** and **I**. N=8 per group for **D** and **F-I.** All error bars represent SEM. Detailed statistical information is shown in Supplementary Table. *P < 0.05, **P < 0.01, ***P < 0.001

Fig. 6

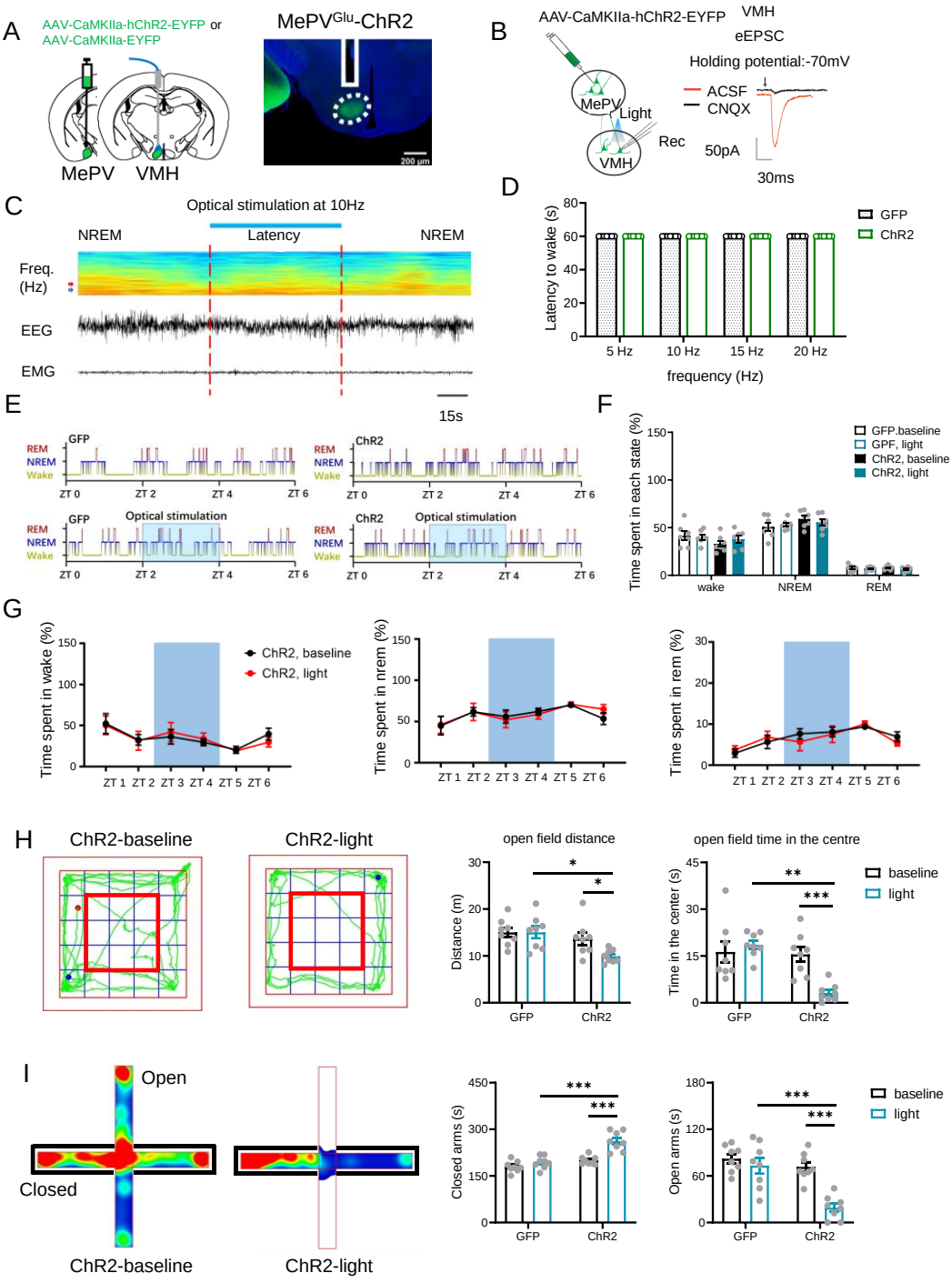

Fig. 6. The role of MePV^{Glu}-VMH pathway on wakefulness and anxiety-like behaviors. A, An optical fiber was implanted into the VMH region of MePV^{Glu}-ChR2 mice to investigate the function of MePV^{Glu}-VMH projection (left). The VMH picture depicted the distribution of ChR2-expressing MePV glutamatergic terminals as well as the placement of optical fiber (right). Scale bar =200 μm. **B,** Patch-

clamp electrophysiology diagram (left). The EPSC was generated by 2 Hz laser stimulation in the VMH as seen by voltage clamp traces (right). **C,** An EEG spectrogram and EEG-EMG trace showed that 10-Hz stimulation was administered during NREM sleep. The arrowheads represent 4 (red) and 8 Hz(blue). The color scale represents the raw power spectral density. Fre., frequency. **D,** Latencies to awaken from sleep following varied frequencies of optical stimulation (The stimulation was performed once per animal; GFP: 8 mice; ChR2: 8 mice). **E,** 2 h optogenetic stimulation hypnograms during the light phase. **F,** Time spent in each state throughout 2 hours of light stimulation. **G,** MePV^{Glu}-VMH-ChR2 mice were subjected to 2 hours of opto-stimulation (10 Hz for 4 seconds with a 56-second interval), and the proportion of waking, NREM, and REM sleep duration. **H,** Representative open field test track plots (left). The open field test involved time spent in the center zone and distance traveled (right). The red frame represents the middle zone. **I,** Heatmaps of the elevated plus maze test (left) and time spent on the open/closed arms (right). Mann-Whitney rank sum test for **D**. Two-way RM ANOVA with Sidak's post hoc comparison for **F**, **G, H** and **I**. All error bars represent SEM. Detailed statistical information is shown in Supplementary Table. **D, F** and **G:** N = 7 per group, **H** and **I:** N = 8 per group. *P < 0.05, **P < 0.01, ***P < 0.001

Fig. 7

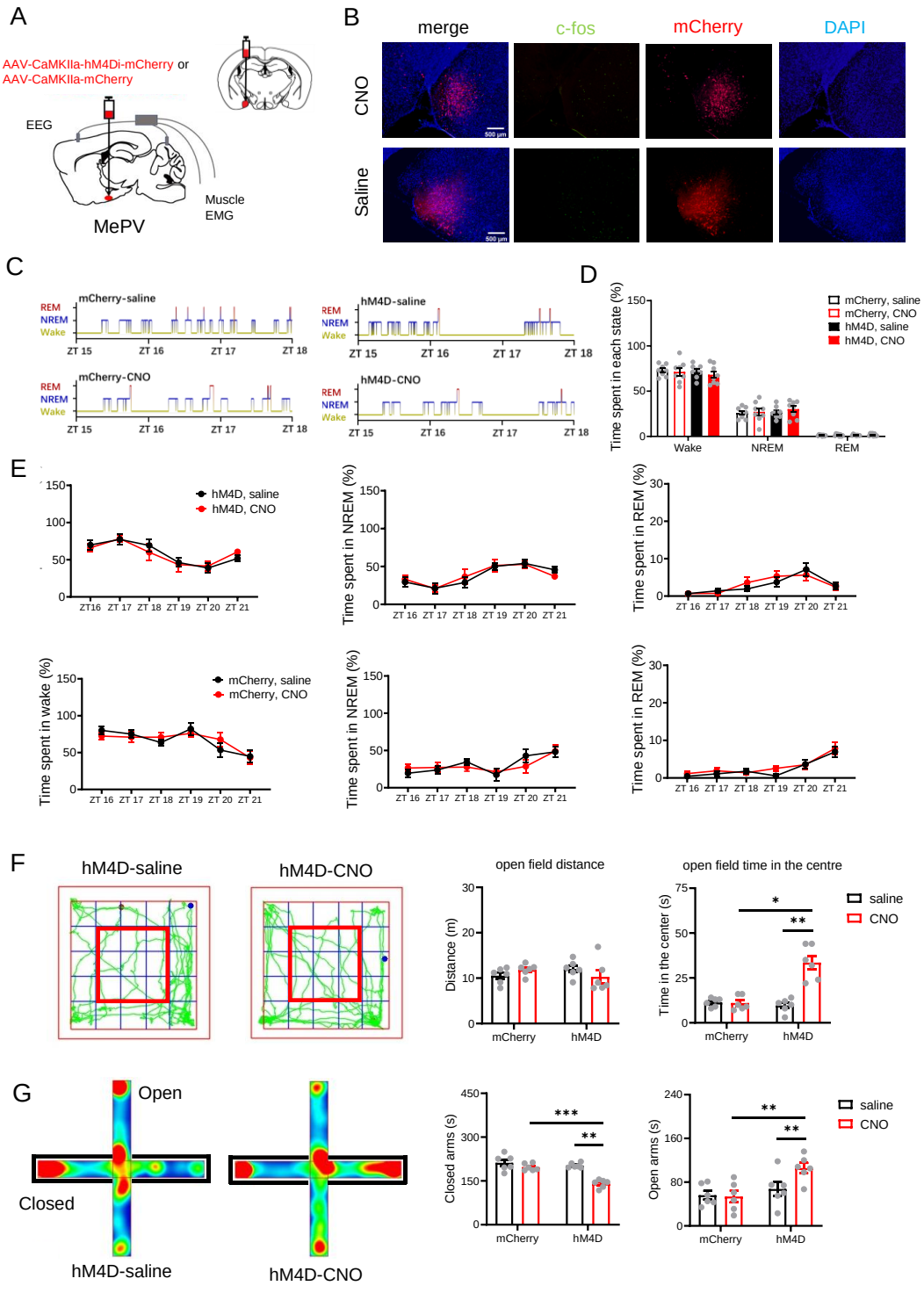

Fig. 7. The effects of chemogenetic inhibition of MePV^{Glu} neurons on wakefulness and anxiety-like behavior. A, Schematic of AAV-CaMKIIa-hM4Di-mCherry/AAV-CaMKIIa-mCherry virus injection and the EEG-EMG recordings. **B,** Representative pictures of c-fos (green), mCherry (red), and DAPI (blue) colocalization in the MePV of hM3Dq mice treated with CNO or saline. Scale bar =500 μm. **C,**

The 3h hypnograms following saline or CNO (1 mg/kg) injections into the AAV-CaMKIIa-mCherry mouse (left panel) and the AAV-CaMKIIa-hM3Dq-mCherry mouse (right panel) (right panel). **D,** Percentages of time spent in each condition for MePV-hM4D and MePV-mCherry mice 3 hours after CNO injection. **E,** The 6h line charts of the AAV-CaMKIIa-hM3Dq-mCherry mouse (top panel) and the AAV-CaMKIIa-mCherry mouse (bottom panel) following saline or CNO (1 mg/kg) injections. **F,** Representative open field test track plots (left). The open field test involved the time spent in the center zone and distance traveled (right). The red frame represents the middle zone. **G,** Heatmaps of the elevated plus maze test (left) and time spent in the open/closed arms (right). Wilcoxon signed rank test, Two-way RM ANOVA with Sidak's post hoc comparison for **D, E, F** and **G**. All error bars are SEM. The detailed statistical data is shown in the supplementary table. **D** and **E:** N = 8 per group, **F** and **G:** N = 6 per group. *P < 0.05, **P < 0.01, ***P < 0.001.

Fig. 8

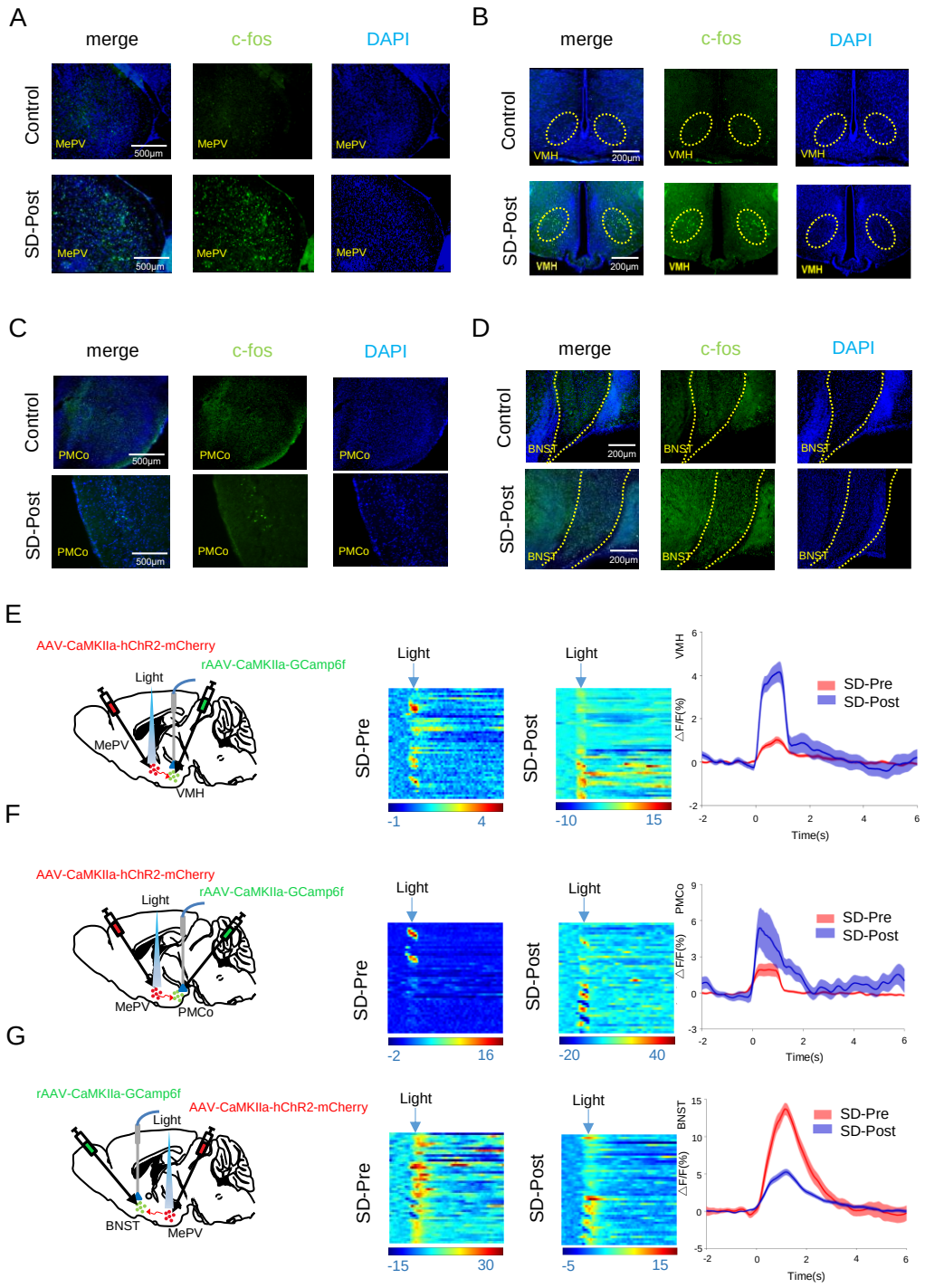

Fig. 8. The effects of sleep deprivation (SD) on the activity of MePV neurons and the MePV-related neuronal circuits. A, The expression of c-fos in the MePV of C57BL/6J mice following a 5-day SD paradigm. Representative immunostaining images of c-fos+ cells in the MePV(A), VMH(B), PMCo(C), and BNST(D) and of Control and SD mice. **E,** Left panel, experimental scheme of bilateral virus injection

into the MePV and VMH. Middle panel, the heat map for the calcium signal of VMH glutamatergic neurons before SD or after SD. The representative transitions (light off-light on) of the changes in color-coded fluorescence intensity before SD or after SD (n=5, 50 trails). Right panel, the mean value (red trace or blue trace) represents the average responses of all the transitions (SEM: red shading or blue shading). **F,** Left panel, experimental scheme of bilateral virus injection into the MePV and PMCo. Middle panel, color-coded fluorescence intensity changes of the representative shifts from the light-off phase to the light-on phase before SD or after SD (n=5, 45 trails). Right panel, the mean value (red trace or blue trace) represents the average responses of all the transitions (SEM: red shading or blue shading). **G,** Left panel, experimental scheme of bilateral virus injection into the MePV and BNST. Middle panel, a shift in color-coded fluorescence intensity illustrates the representative transition from the light-off phase to the light-on phase before SD or after SD (n=5, 47 trails). Right panel, the mean value (red trace or blue trace) represents the average responses of all the transitions (SEM: red shading or blue shading). Data are presented as mean ± SEM.

Fig. 9

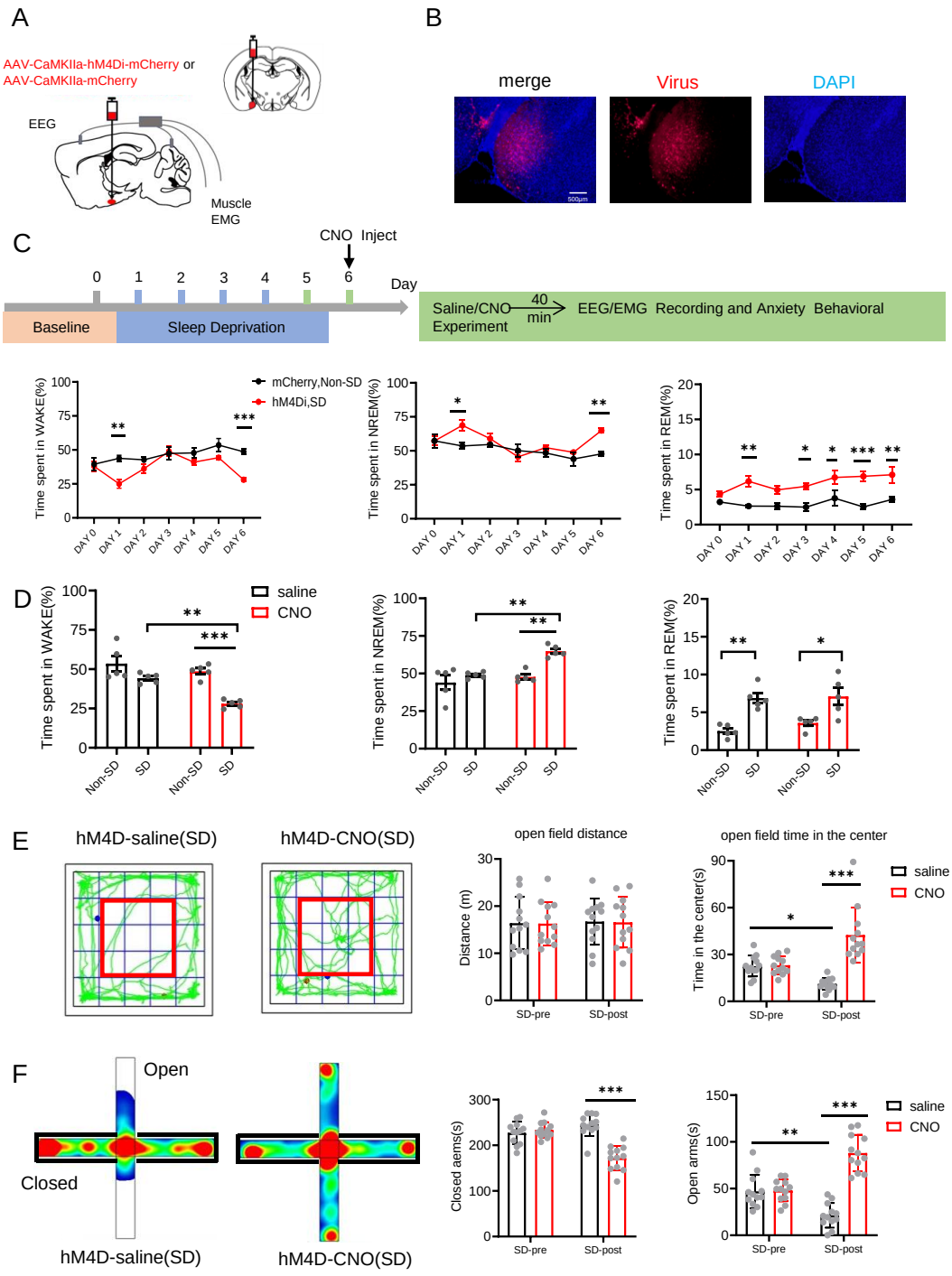

Fig. 9. Inhibiting MePV^{Glu} neurons with a chemogenetic agent decreased wakefulness and induced an anxiolytic effect on the mice treated with SD. A, Schematic of AAV-CaMKIIa-hM4Di-mCherry/AAV-CaMKIIa-mCherry virus injection and the EEG-EMG recordings. **B,** Representative pictures of virus (red), DAPI (blue) and colocalization in the MePV of hM3Dq mice. **C.** Upper panel,

schematic diagram of the experimental process. Mice were subjected to sleep deprivation from Day 1 to Day 5. On Day 6, mice were given saline or CNO separately. We recorded and examined EEG and EMG data for 6 hours immediately after the sleep deprivation or the CNO treatment (n = 5 mice). Lower panel, the statistical analysis results of wakefulness time, NREM sleep time and REM sleep time for 6 days. **D,** The statistical analysis results of wakefulness time, NREM sleep time and REM sleep time on Day 6 (n = 5 mice). **E,** Representative traces of open field test (left). The red frame represents the middle zone. The statistical analysis results of open field tests involved distance traveled and the time spent in the center zone (right) (mCherry: n = 12 mice; hM4Di: n = 12 mice). **F,** Heatmaps of the elevated plus maze test (left) and time spent on the EPM open/closed arms (right). Statistical significance was determined using the two-way RM ANOVA. Data are presented as mean ± SEM. *P < 0.05, **P < 0.01, ***P < 0.001.